KONA Powder and Particle Journal

KONA Powder and Particle Journal No. 42 (2025) 134–155/https://doi.org/10.14356/kona.2025011 Review Paper

Progress in the Application of Multidimensional Particle Property Distributions: The Separation Function †

Edgar Schach [1], Thomas Buchwald [1], Orkun Furat [2], Florentin Tischer [3], Alexandra Kaas [1], Laura Kuger [4], Matthias Masuhr [5], Johanna Sygusch [6], Thomas Wilhelm [2], Ralf Ditscherlein [1] and Urs Alexander Peuker [1]*

[1] *Institute of Mechanical Process Engineering and Mineral Processing, TU Bergakademie Freiberg, Germany*
[2] *Institute of Stochastics, Ulm University, Germany*
[3] *Department of Chemical and Biological Engineering, Friedrich-Alexander-Universität Erlangen-Nürnberg, Germany*
[4] *Institute of Functional Interfaces, Karlsruhe Institute of Technology, Germany*
[5] *Institute of Technology for Nanostructures, Universität Duisburg-Essen, Germany*
[6] *Helmholtz Institute Freiberg for Resource Technology, Helmholtz-Zentrum Dresden-Rossendorf, Germany*

In KONA 2022, the fundamentals of two- and multidimensional particle size distributions were introduced. The next question in the field of two- and multidimensional distributions addresses their application to describe a particle process, e.g., agglomeration or separation. A multidimensional separation can be seen as retrieving only particles with a specific set of properties from a multidimensionally distributed system, e.g., retrieving only small particles (below a certain threshold in size) with a compact spherical shape (above a certain threshold in sphericity). The multidimensional separation allows the generation of functional particle systems with specific properties, e.g., semiconducting, optical, or electronic properties, which are required for high-technology applications. Starting from so-called particle-discrete information, i.e., an information vector for each particle containing its compositional, geometrical, and physical properties, it is possible to describe a multidimensional separation in full detail based on various properties. Each particle can be evaluated according to different separation properties, e.g., size, shape, and material composition. With this database, it is possible to define and work with separation functions to describe the multidimensional separation and quantify the separation results. For example, in the two-dimensional case, the median cut size becomes a median cut line, where the probability for a particle to belong to the concentrate is 0.5. Some case studies and examples show different approaches and possibilities to achieve a multidimensional separation in one or several connected process steps.

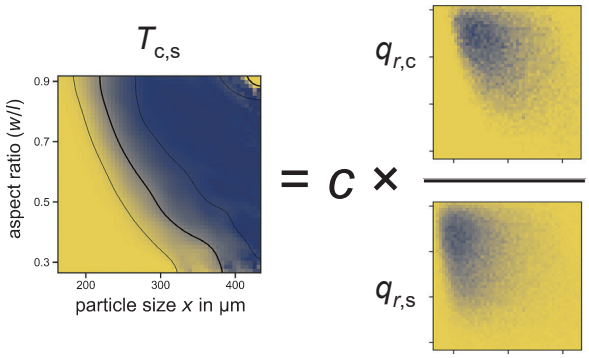

Keywords: separation function, Tromp curve, partition curve, multidimensional, particle property distribution

1. Introduction

In KONA 2022, Frank et al. presented the fundamentals of two- and multidimensional particle size distributions, allowing for a more detailed description of particle systems than combining a constant shape factor with a particle size distribution. They also demonstrated the challenges in measuring and retrieving multidimensional particle size distributions (Frank et al., 2022). Particle-discrete information is necessary to generate particle property distributions of any dimension. For the one-dimensional distribution, which we all know as particle size distribution (PSD), the starting point is the information about the size, i.e., the equivalent diameter, of each discrete particle. This information is grouped into size classes and weighted by number, cord length, surface, or volume. To compute particle property distributions of higher dimensions, which show the distributed values of size, shape, composition, crystallinity, and others simultaneously, particle-discrete information has to be extracted (**Fig. 1**). Thus, each particle is described by an information vector containing the relevant particle-discrete data of its properties.

In addition to the multidimensional information about particle geometry, the composition of the individual particles provides additional dimensions in the description of particle systems. These dimensions are central aspects in the field of primary and secondary raw materials, where ores, slags, or anthropogenic waste materials (**Fig. 2**) have to be characterized, processed, and separated (Werner et al., 2020). Individual multicomponent particles are intergrown, i.e., they have a complex microstructure consisting of more than one material phase.

The cassiterite ore shown here (**Fig. 3**) consists of four

† Received 29 June 2023; Accepted 6 October 2023
J-STAGE Advance published online 29 June 2024
* Corresponding author: Urs Alexander Peuker;
Add: Agricolastraße 1, KKB-1057, 09599 Freiberg, Germany
E-mail: urs.peuker@mvtat.tu-freiberg.de
TEL: +49-3731-39-2795

main materials, i.e., minerals. Each particle within the ore sample is composed of one or more of these minerals. Material classes are chosen to reduce complexity, i.e., the dimension of the problem. For example, all iron-containing phases are grouped together in the material class iron oxides. Using the color code, it becomes apparent that there is a vast diversity among the individual particles, even with just four different material phases. This behavior is also observed in the slag sample in **Fig. 3 (right)**, which exhibits multiple material phases.

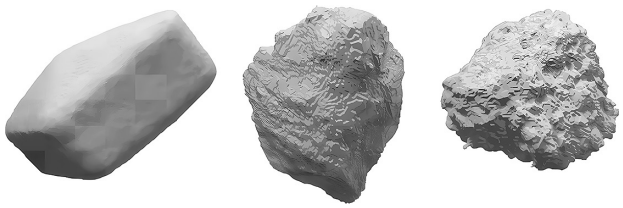

Fig. 1 3D particles of different materials from which geometrical data can be retrieved, determined by 3D scanning **(left)** and by µ-CT **(middle and right)**.

Fig. 2 Particles from the mechanical recycling process of lithium-ion-batteries as explained in Ref. (Werner et al., 2020), showing particles with non-compact irregular and significantly distributed shape properties.

Multimaterial particles also become increasingly important in the field of particle design, when particles are coated (**Fig. 4**), encapsulated, co-precipitated, or integrated into composite materials (Hickstein and Peuker, 2009). The interplay between different properties of a particle collective has therefore come into focus of research in recent years (Bagheri et al., 2015).

In summary, the concept of particle-discrete information forms the basis for generating multidimensional particle property distributions. These distributions are created by constructing property vectors for individual particles, which include various properties such as characteristic length, volume, shape factor, composition, porosity, roughness, and crystallinity. The more elements are included in the vector, the higher becomes the potential dimensionality of the property distribution that can be generated from the particle-discrete data set. Common measuring techniques producing particle-discrete, multidimensional data are computed tomography (Çiçek et al., 2016; Ditscherlein et al., 2020; Egan et al., 2015; Leißner et al., 2020), dynamic image analysis (Bujak and Bottlinger, 2008; Kuzmanić and Mikoš, 2022; Oliver et al., 2019), and mineral liberation analysis (Leißner et al., 2016), as shown in **Fig. 3**. Other measuring techniques in which multidimensionality poses a particular problem include the shape influence in laser diffraction analysis (Matsuyama and Yamamoto, 2005; Peciar et al., 2022).

The properties in the vector may originate from different sources. Initially, these are the original measurement data obtained from different characterization methods and principles. It is crucial to ensure that the data is thoroughly linked to the corresponding particle when combining or correlating measurements from different principles. Some properties in the vector, such as equivalent diameters and shape factors, are calculated or aggregated parameters (Heywood, 1961). These properties can be added to the

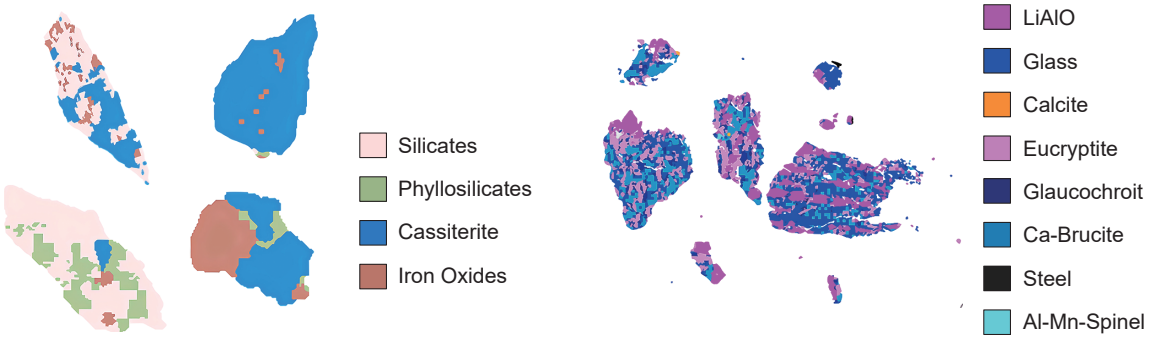

Fig. 3 Material-related properties of individual particles, measured by mineral liberation analysis (MLA), which is a SEM-EDX-system, coupled with a mineral data base. Adapted with permission from Ref. (Buchmann et al., 2020b). **Left**: particles from different material streams in the processing of a cassiterite ore (Ehrenfriedersdorf, Saxony); **right**: particles from a lithium-aluminate slag (RWTH Aachen IME), which occurs in lithium-ion-battery recycling.

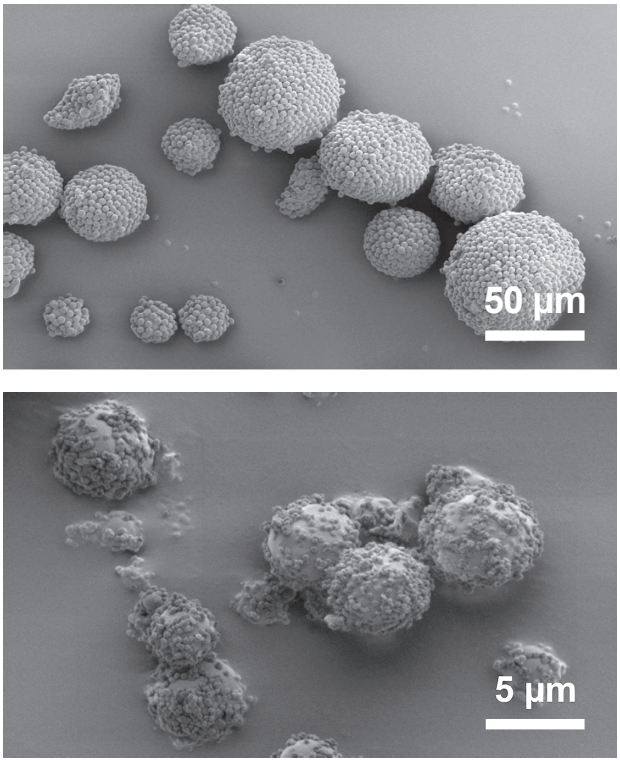

Fig. 4 SEM pictures of surface coated particles. The particles were produced by mechano-fusion (Alonso et al., 1989; Pfeffer et al., 2001; Tanno, 1990). **Top**: carrier particle (Al_2O_3 - DAW-45, Denka) with a polystyrene particle coating (Chemisnow SX-350 H, Soken Chemical); **bottom**: carrier particles (Alumina - DAW-05, Denka) coated with PMMA (Chemisnow MP2801, Soken Chemical) (Friebel et al., 2024).

vector, resulting in a rapid increase in the number of elements. From the methodological perspective, particle-discrete multidimensional data sets are essential for creating multidimensional property distributions since they contain all necessary information. Only with additional information or assumptions, such as precise knowledge of particle geometry in the case of synthesized nanoparticles, it is possible to directly generate the corresponding unique multidimensional distribution from several one-dimensional distributions (marginal distributions) (Demeler et al., 2014). Imaging techniques and correlative imaging methods, such as X-ray computed tomography, are often preferred for generating particle-discrete data sets (Frank et al., 2019; 2022).

The multidimensional description of the particle collective then provides the methods to investigate many common separation processes. On most classification and sorting machines, particles are sorted according to more than one parameter. While some of these properties are perceived to have an influence, they have yet to be thoroughly investigated. A perfect example is the sieving process, in which results are displayed as a separation according to particle size, but where particle shape plays a vital role (Blott and Pye, 2008; Dehghani et al., 2002; Nakajima et al., 1979; Whiteman and Ridgway, 1986). Other examples are sedimentation (Wadell H., 1932a,b; 1933) and the aero- (Furchner and Zampini, 2009), and hydrodynamic separation processes (Fontein, 1961), as well as processes for shape separation (Furuuchi and Gotoh, 1992).

Often, the multidimensionality of a separation process is implicitly shown by researchers without highlighting the multidimensionality explicitly (Tang and Puri, 2007). Examples include the separation of PET flakes from plastic bottle recycling on zig-zag sifters and air jigs (Friedländeret al., 2006) and separation by thermo-adhesion, where particles are selectively heated by microwaves until they stick to a surface (Baloun. et al., 2005).

In other separation processes, most importantly some analytical methods, the multidimensionality of the separation process is of key interest, for example, in flow-field fractionation, where particles are separated hydrodynamically inside a flat channel (Baalousha et al., 2011). Recently, separation processes have been shown to become comparable by calculation of a statistic entropy that describes the degree of disorder in a particle collective (Buchmann et al., 2020a).

In the following, a description of multidimensional particle property distributions is given, followed by a description of how two-dimensional separation processes can be presented in a convenient manner. The text ends with a review of some examples of multidimensional separation.

2. Theoretical background

2.1 Working with particle-discrete datasets

When particle-discrete datasets are available, it is possible to generate the corresponding multidimensional particle property distributions. As in the one-dimensional case, property classes are defined with appropriate boundaries. In the multidimensional case, a property class addresses more than one property (**Fig. 5**). For the two-dimensional example, with the properties x (equivalent diameter/particle size) and y (shape factor), each class contains the fraction of all particles, which fulfill the specifications:

- equivalent diameter: $x_{i-1} < x \leq x_i$
- shape factor: $y_{j-1} < y \leq y_j$

The two-dimensional particle density distribution uses a definition similar to the one-dimensional case. The following example considers a set of particle data in which the volume of each particle is known. Only under the assumption of constant density, a volume- or mass-weighted distribution can be computed. Where length- and area-based distributions will sometimes occur in the description of one-dimensional property distributions, in practice, multidimensional distributions will either be number- or volume-/mass-weighted.

To obtain the two-dimensional density distribution, the mass of the particles in class $[i, j]$, $m_{i,j}$, is divided by the

overall mass m_{total} and the area of that class, which now involves two dimensions, Δx_i for the property x and Δy_j for the property y:

$$q_3\left(\overline{x}_i, \overline{y}_j\right) = \frac{m_{i,j}}{m_{\text{total}}\ \Delta x_i\ \Delta y_j} = \frac{\Delta Q_{3,i,j}}{\Delta x_i \Delta y_j} \tag{1}$$

The width of the property classes is the difference between the upper and lower limits for each property:

$$\Delta x_i = x_i - x_{i-1} \tag{2}$$
$$\Delta y_i = y_j - y_{j-1} \tag{3}$$

Using dx and dy for the size of the classes, the two-dimensional property distribution can be written in a differential form as well:

$$q_3(x,y) = \frac{\mathrm{d}^2 Q_3}{\mathrm{d}x\mathrm{d}y} \tag{4}$$

The normalization condition that the sum or the integral of a density distribution is equal to one is also valid for the two- and multidimensional cases. In the two-dimensional case, the density distribution has to be summed up over both x and y:

$$\sum_{j=1}^{m}\sum_{i=1}^{n} q_3(x_i, y_j) = 1 \tag{5}$$

The definition range of a two-dimensional property distribution describes a defined area in the x-y-plane. Outside this area, the density distribution is by definition:

$$q_3(x,y) = 0 \quad \text{if } x \le x_{\min} \text{ and / or } y \le y_{\min} \tag{6}$$
$$q_3(x,y) = 0 \quad \text{if } x > x_{\max} \text{ and / or } y > y_{\max} \tag{7}$$

The cumulative sum is calculated via summing up or integrating the density distribution from the minimal values $x_{\min}$ and $y_{\min}$ up to a point (x, y):

$$\begin{aligned} Q_{3,i,j} &= \sum_{\mu=1}^{j}\sum_{\nu=1}^{i} \Delta Q_{3,\nu,\mu} \\ &= \sum_{\mu=1}^{j}\sum_{\nu=1}^{i} q_{3,\nu,\mu}\, \Delta x_\nu\, \Delta y_\mu \end{aligned} \tag{8}$$

$$Q_3(x,y) = \int_{y_{\min}}^{y}\int_{x_{\min}}^{x} q_3(x,y)\mathrm{d}x\mathrm{d}y \tag{9}$$

For the two-dimensional case, the cumulative sum is zero when both properties are below their minimal values and is 1 if both properties are above their maximum value:

$$Q_3(x,y) = 0 \quad \text{if } x \le x_{\min} \text{ or } y \le y_{\min} \tag{10}$$
$$Q_3(x,y) = 1 \quad \text{if } x > x_{\max} \text{ and } y > y_{\max} \tag{11}$$

For better visualization heat plots, which project the third dimension, i.e., the numerical value of the distribution, in a color code, should be used instead of the 3D-plots (**Fig. 6**). For example, **Fig. 7** shows the same two-dimensional data-set (**Fig. 6, right**) as a heat map. Of course, this type of visualization can also be implemented for the density distribution (**Fig. 6, left**).

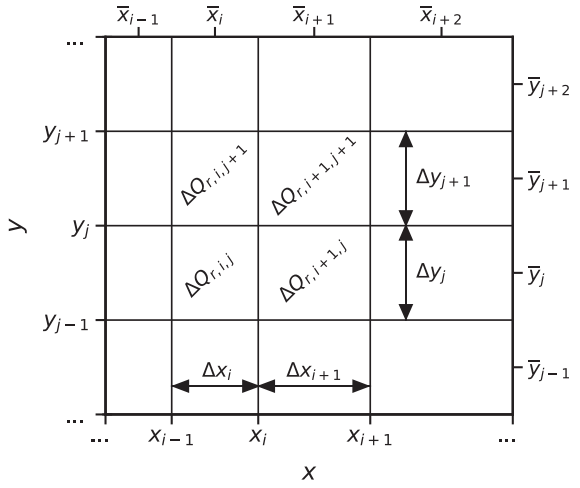

Fig. 5 Schematic representation of the two-dimensional definition of property classes for the properties x and y.

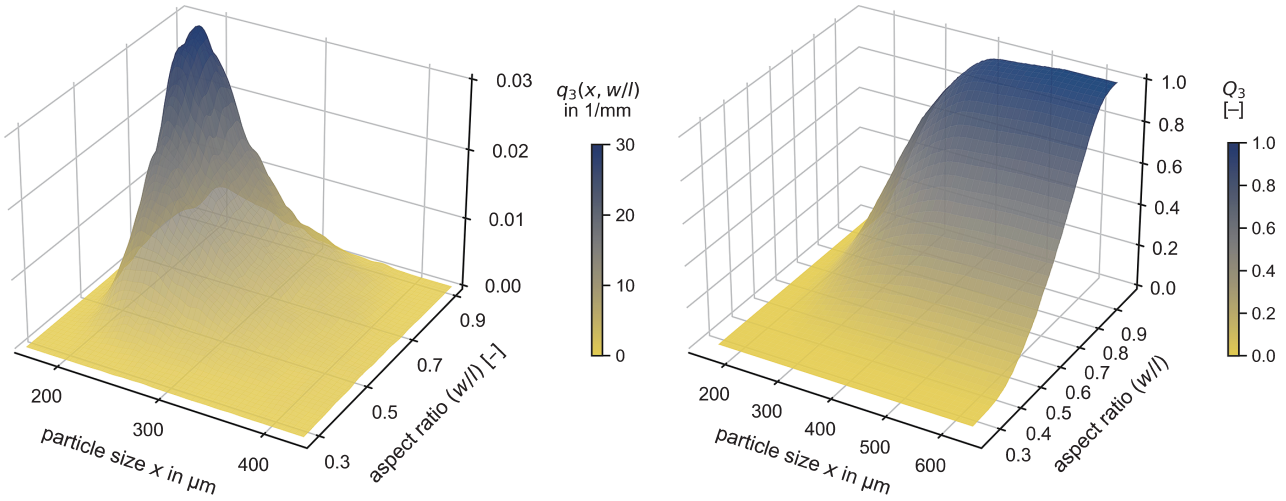

Fig. 6 3D-plot of a two-dimensional size-shape-distribution of 56500 particles, measured with the dynamic image analysis system PartAn 3D; **left**: probability density function; **right**: cumulative sum.

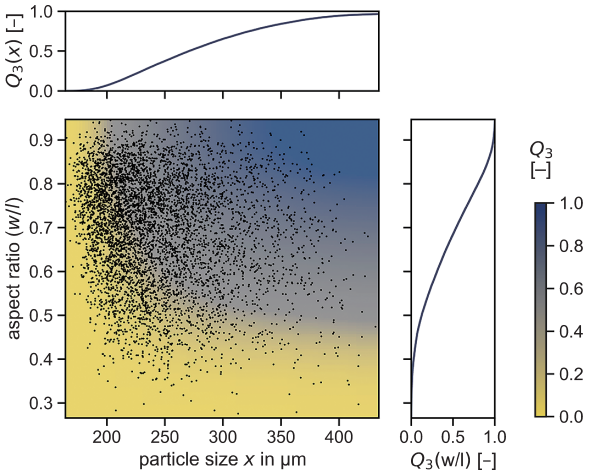

Fig. 7 Two-dimensional plot of the cumulative sum (mass-weighted), also displaying the discrete particles' data points. The outer one-dimensional distributions are the corresponding marginal distributions for size x and aspect ratio $y = w/l$.

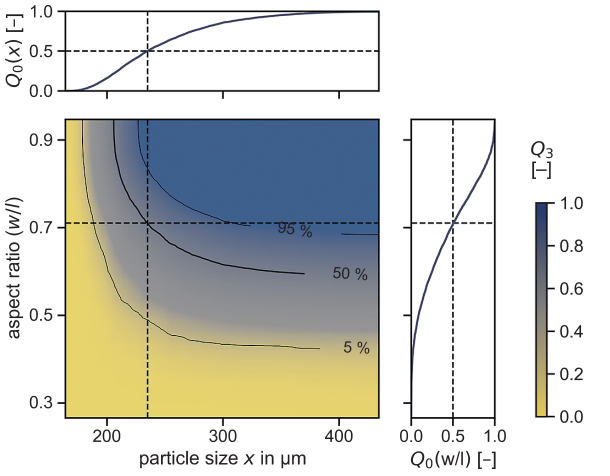

Fig. 8 Cumulative sum distribution showing the isolines for 5 %, 50 %, and 95 %. Visualization of the median particle size (x_{50}, y_{50}) as the intercept of the median values of the marginal distributions.

Marginal distributions are distributions of lower dimensionality. For the exemplary two-dimensional case (x, y), the corresponding marginal distributions are the one-dimensional distributions of the individual properties x and y. These derive from an integration over the other property, i.e., for $q_3(x)$ derives from $q_3(x, y)$ as integration over y in the entire variable range y_{min} to y_{max}:

$$q_3(x) = \int_{y_{min}}^{y_{max}} q_3(x, y)\,\mathrm{d}y \tag{12}$$

$$q_3(y) = \int_{x_{min}}^{x_{max}} q_3(x, y)\,\mathrm{d}x \tag{13}$$

The marginal one-dimensional distributions can be visualized at the individual axis of the heat-plot of the two-dimensional distribution (**Fig. 7**), either as histograms for discrete property classes or as smooth functions, when the heat plot shows a differential presentation of the distribution. The latter typically uses an interpolation between the property classes or even between the individual data points. Suitable interpolation methods are kernel density estimation (Schach et al., 2019) and copulas (Czado, 2019; Furat et al., 2019; Joe H., 2014).

2.2 Characteristic particle sizes of the multidimensional distribution

One-dimensional particle size distributions are commonly described by the median particle size or the modal particle size as characteristic values, which are used to represent the entire particle size distribution with a single parameter, e.g., in empirical models. The identification of the modal particle property within the two- or multidimensional property distribution is quite simple, since the modal property is the peak in the 3D plot, i.e., the element of the multidimensional property matrix (**Fig. 5**) with the highest numerical value. Regarding the complexity of the multidimensional property distributions, multimodal distributions (with several distinct peaks) are expected to occur much more frequently than in the one-dimensional case.

The definition of the median particle property requires a detailed view of the distribution itself. In the two-dimensional case, there is an isoline, which contains all points that split the particle system into two fractions of same quantity. For example, in **Fig. 8**, which shows the distribution by number, 50 % of the particles derive from a fraction with an aspect ratio below 0.63 and particle-equivalent diameter below 350 µm; however, 50 % of particles are also contained in the fraction of particles below an aspect ratio of 0.8 and a particle-equivalent diameter of 230 µm and smaller. The isoline itself cannot serve as one single characteristic parameter, but it is clear that the median of the cumulative sum of this particle system is located on this isoline. For the definition of the median particle size of a two-dimensional particle property distribution, we look at the intercept of the marginal property distributions. The median (x_{50}, y_{50}) is the point which fulfills the following two conditions:

1. 50 % of the particles originate from particles below this size, which is the x_{50} of the marginal size distribution.
2. 50 % of the particles originate from particles below this shape factor, which is the y_{50} of the marginal shape distribution.

Looking at the heat plot with the curved and monotonically decreasing isoline (**Fig. 8**), the median represents in the two-dimensional case the point that creates the rectangle having the maximum area A. Thus, the median (x_{50}, y_{50}) additionally fulfills the following condition:

$$A = (x_{max} - x_{50})(y_{max} - y_{50}) = \max. \tag{14}$$

3. Fundamentals of mixing and separation of multidimensionally distributed particle systems

Having defined the multidimensional property distribution, it has to be investigated how they can be used to describe particle-based processes.

3.1 Mixing of particle collectives

The mixing of two or more multidimensionally distributed particle systems still follows a simple mass balance, e.g., for the mixture of two samples:

$$m_{\mathrm{res}} = m_1 + m_2 \tag{15}$$

Using the relative mass v, i.e., the mass fraction, allows for a normalized discussion of the mixing process, where all relative masses v_i sum up to one:

$$v_1 = \frac{m_1}{m_{\mathrm{res}}} \tag{16}$$

$$v_2 = \frac{m_2}{m_{\mathrm{res}}} \tag{17}$$

$$v_1 + v_2 = 1 \tag{18}$$

The resulting probability density distribution of the mixture can then be calculated from the density distributions of the individual samples:

$$q_{\mathrm{res}}(x,y) = v_1 q_1(x,y) + v_2 q_2(x,y) \tag{19}$$

$$Q_{\mathrm{res}}(x,y) = v_1 Q_1(x,y) + v_2 Q_2(x,y) \tag{20}$$

It has to be stated that it is only possible to mix particle property distributions of the same dimension, i.e., the particle property distribution of the mixture will have the dimensions of the particle property distribution with the lowest dimensionality.

When a three-dimensional property distribution is mixed with a two-dimensional distribution, the three-dimensional distribution has to be marginalized to a two-dimensional distribution prior to the calculation of the mixing process. Consider, for example, a dataset in which a multidimensional distribution of particle size, shape, and density is known. For the second product, density was not determined explicitly. In calculating the probability density of the resulting mixture, the information on density is lost. The marginalization therefore leads to a loss in information, which cannot be reversed later on, unless the resulting distributions are measured again.

The generalized form, which describes the mixing of n different distributions with the dimensionality m, is the weighted sum of the n distributions:

$$q_{\mathrm{res}}(x_1,\ldots,x_m) = \sum_{i=1}^{n} \left(v_i\, q_i(x_1,\ldots,x_m)\right) \tag{21}$$

3.2 Multidimensional separation function / Tromp curve

A multidimensional separation is defined as a separation according to more than one property. Independent of the dimensionality of the feed, the separation step creates two product fractions that vary in more than one property. Since this separation is not only a separation according to size parameters, the nomenclature of "concentrate" (c; mass fraction of concentrate) and "reject" (r; mass fraction of retentate) is used for the two product fractions, the first containing the product (valuable material), the latter containing particles of lesser interest. The indices are derived from the sorting nomenclature with C for "concentrate" and R for "refuse" or "reject". Correspondingly, the index S is used for the feed material ("supply") (c.f. ISO 9276-4).

As an example, for the two-dimensional case, the mass balance of the distribution densities can be written using the corresponding mass fractions:

$$1 = \frac{m_{\mathrm{C}}}{m_{\mathrm{S}}} + \frac{m_{\mathrm{R}}}{m_{\mathrm{S}}} = c + r \tag{22}$$

$$q_{\mathrm{S}}(x,y) = c\, q_{\mathrm{C}}(x,y) + r\, q_{\mathrm{R}}(x,y) \tag{23}$$

The correlation of the integral mass balance and the class-wise mass balance allows for the recalculation of the concentrate and reject mass fractions using the data from the three density distributions involved in the separation, i.e., supply, concentrate, and reject:

$$c = \frac{q_{\mathrm{S}}(x,y) - q_{\mathrm{R}}(x,y)}{q_{\mathrm{C}}(x,y) - q_{\mathrm{R}}(x,y)} \tag{24}$$

$$r = \frac{q_{\mathrm{S}}(x,y) - q_{\mathrm{C}}(x,y)}{q_{\mathrm{R}}(x,y) - q_{\mathrm{C}}(x,y)} \tag{25}$$

The separation function T indicates the probability whether a particle will be transferred to the concentrate or stay in the reject. The separation function T is defined in the interval [0, 1]. If the function equals $T = 1$, then the feed with these properties is entirely discharged into the concentrate. If it equals to $T = 0$, the concentrate fraction contains no particles from the feed in that area, and all feed material is discharged into the reject. Values of the separation function between 0 and 1 are a measure of the probability of the feed material ending up in the concentrate in a specific interval.

Since the degree of separation is the fraction of the particle mass in each class (i, j) that passes into the concentrate fraction, it can also be calculated from the respective distribution densities for the two-dimensional case. The calculation of the degree of separation for the higher-dimensional cases requires three discrete pieces of information, either all three property distributions of feed (s), concentrate (c) and reject (r), or two property distributions and a mass ratio c or r.

Like the one-dimensional separation functions, the multidimensional separation function has a definition range in

which they can take values between 0 and 1, in which the separation is subject to a degree of uncertainty. This definition range is for $T(x, y)$ in the range between x_{min} and x_{max} as well as between y_{min} and y_{max}. However, individual classes in this two-dimensional area can take the values 0 or 1, because for them a complete separation into concentrate or reject can occur. Furthermore, the calculation of $T(x, y)$ can give values outside the definition range of 0 and 1. The reason for such values is, in most cases an erroneous balance between the products and the feed material. An appropriate mass balance of the particle classes might be necessary to obtain reasonable results as e.g., proposed by Lamberg et al. (Lamberg and Vianna, 2007). Furthermore, balances can be biased due to analytical errors, which might require a correction of the results (Buchmann et al., 2018).

If one defines the two-dimensional separation function on the basis of the associated two-dimensional density distributions of feed material and concentrate and the mass balance, it leads to the separation function $T_{SC}(x, y)$:

$$T_{SC}(x,y) = \frac{c\,q_C(x,y)}{q_S(x,y)} \tag{26}$$

Using the mass balance to replace $c\,q_C(x, y)$ with $q_S(x, y) - r\,q_R(x, y)$, a different definition of the separation function is obtained, which uses the information of the reject and feed material:

$$T_{SR}(x,y) = \frac{q_S(x,y) - r\cdot q_R(x,y)}{q_S(x,y)} = 1 - r\frac{q_R(x,y)}{q_S(x,y)} \tag{27}$$

The marginal separation function is a lower-dimensional separation function of a multidimensional separation function. For the two-dimensional case, the one-dimensional separation function, i.e., a Tromp curve, is the corresponding marginal separation function. For each two-dimensional partition function there are two marginal distributions, each of which represents the one-dimensional partition function with respect to the associated property:

$$T_{SC}(x) = c\cdot\frac{\int_{y_{min}}^{y_{max}} q_C(x,y)\,dy}{\int_{y_{min}}^{y_{max}} q_S(x,y)\,dy} \tag{28}$$

$$T_{SC}(y) = c\cdot\frac{\int_{x_{min}}^{x_{max}} q_C(x,y)\,dx}{\int_{x_{min}}^{x_{max}} q_S(x,y)\,dx} \tag{29}$$

4. Separation functions

Before discussing the model cases of multidimensional separation, the one-dimensional separation function (Tromp curve) for a classification step is depicted in **Fig. 9 (left)**. The graph shows the distribution of the fine (f) and coarse (c) material, weighted by the mass split of the separation, the resulting Tromp curve with a typical sigmoidal shape and the separation cut size (x_T).

Because it will be an effect in the following discussion, **Fig. 9 (right)** shows a Tromp curve that exhibits the well-known fishhook, starting at values greater than 0. There are different explanations for such a process behavior, including, e.g., entrainment, adhesion of fine particles on coarse particles or measurement errors (Bourgeois and Majumder, 2013; Nageswararao, 2000).

4.1 Examples of separation functions

Buchwald et al. (2023) discussed the deduction of the two-dimensional separation function for a virtually separated particle system, where the particle-discrete data on the equivalent particle diameter and the shape factor aspect ratio were known. In that paper, the dataset coming from a dynamic image analysis (PartAn 3D) was presented as a mass distribution with a low resolution using 6 × 6 property classes. Increasing the resolution to 50 × 50 property classes provides a smoother view of the same dataset and allows for a more accurate description of the separation function with isolines. Furthermore, some special details of the separation become visible, e.g., the two-dimensional equivalent of the fishhook effect.

4.2 Model cases of separation

To evaluate and classify a two- or higher-dimensional separation function, it is necessary to discuss the model cases of a two-dimensional separation (**Fig. 10**). Starting with the presentation of the ideal one-dimensional separation in the two-dimensional plot, the heat plot shows either

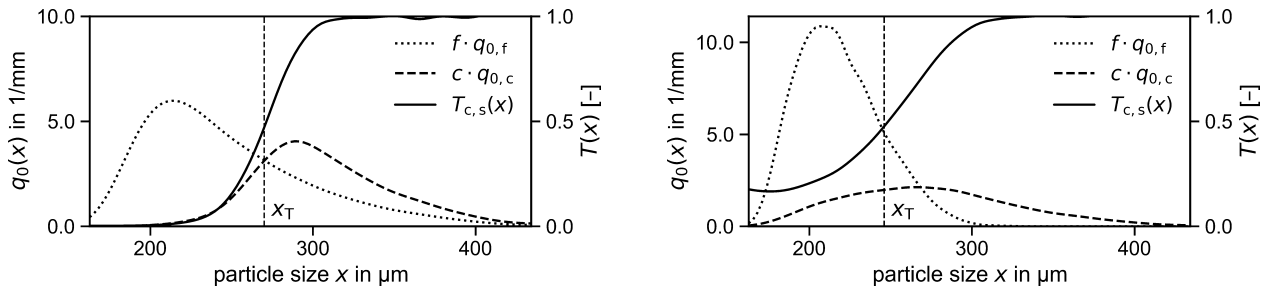

Fig. 9 Two one-dimensional separation functions for size separations (classifications) with the underlying density functions of both the fine and the coarse fractions. The density functions have been multiplied by the respective mass fraction to better represent the mass share graphically. **Left**: ideal separation function of sigmoidal shape; **right**: separation function with "fishhook".

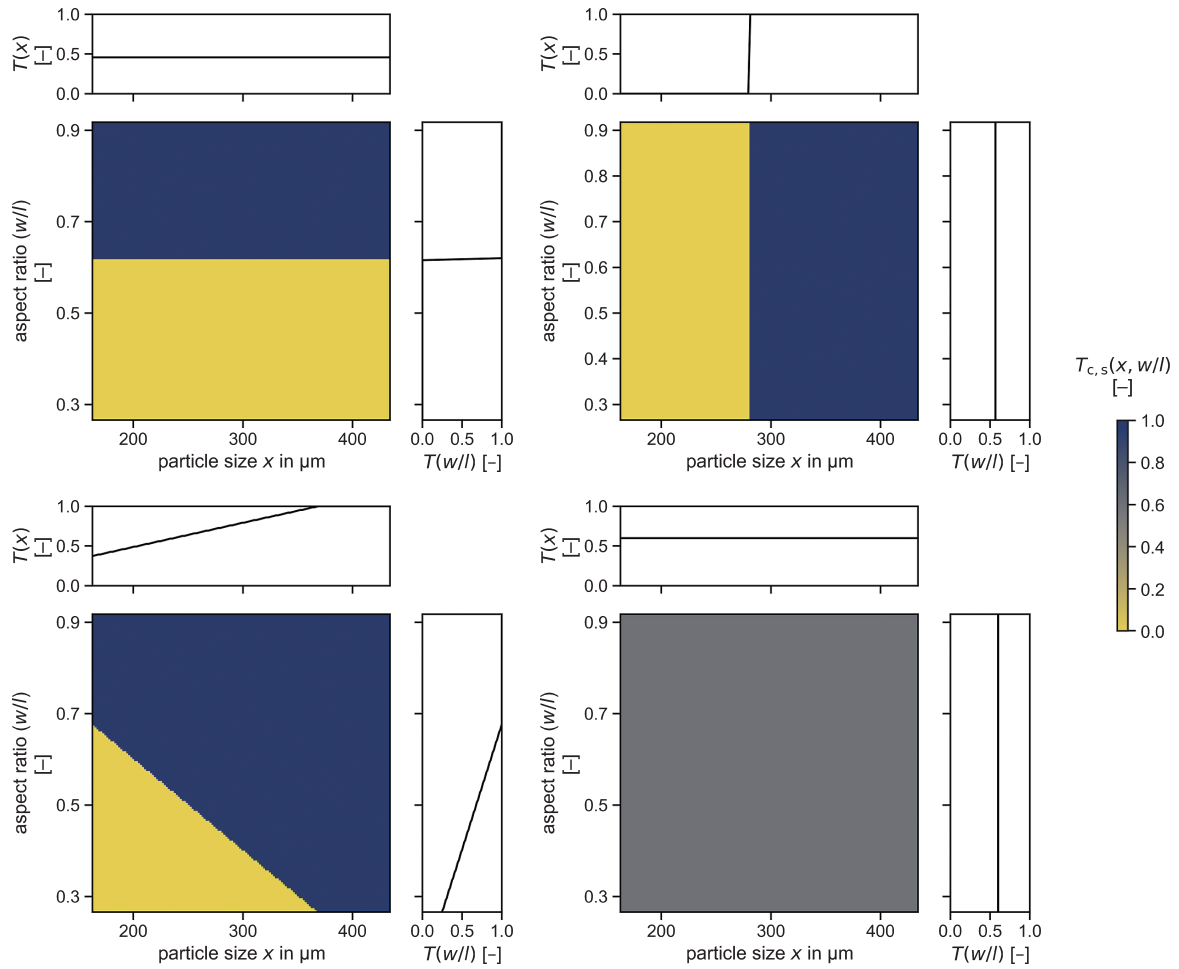

Fig. 10 Ideal cases of the two-dimensional separation function for the parameters x (size) and $y = w/l$ (aspect ratio); **upper left**: ideal one-dimensional separation according to aspect ratio; **upper right**: ideal one-dimensional separation according to particle size; **lower left**: two-dimensional separation according to a linear combination of both parameters; **lower right**: ideal splitting without any influence of either size or aspect ratio.

a horizontal (**Fig. 10, upper left**) for a separation only according to the particle aspect ratio, with the reject at the bottom and the concentrate on the top, or a vertical isoline for the separation (**Fig. 10, upper right**) with the reject on the left and the concentrate on the right. Because the separation is only due to a single parameter, the marginal separation function of this parameter will show the step function of an ideal separation function, whereas the other marginal separation function will exhibit the behavior of ideal splitting with a constant value over the entire parameter range.

A perfectly sharp separation that involves both parameters separates the parameter field into two areas of concentrate and reject (**Fig. 10, lower left**). The concentrate is situated in the upper right part of the plot, whereas the reject is found in the lower left. Even though the two-dimensional separation function shows a perfectly steep increase, the marginal one-dimensional separation functions show imperfectness: both marginal separation functions increase from a starting value above zero and reach one within the definition range of the particle property distribution. This effect can be described as fishhook, as briefly explained in **Section 3.2**. The multidimensional case in **Fig. 10** shows that fishhook effects in the one-dimensional margin distributions might be caused by an underlying multidimensional behavior. This effect can be found, e.g., for separation processes in fluid flows, in which, in addition to size and shape, the particle density has an impact on the particle process response.

The case of perfect splitting (**Fig. 10, lower right**), where feed, concentrate, and reject have an identical particle property distribution, results in a homogenous color over the entire definition range of the separation function in the heat plot.

4.3 Application of model cases

Particles were analyzed by dynamic image analysis in the PartAn 3D (now Camsizer 3D) by Microtrac. The device tracks particles while they fall through the measuring window, which allows for a recreation of the 3D appearance of the particle from several rotated views. In contrast to conventional dynamic image analysis, which solely

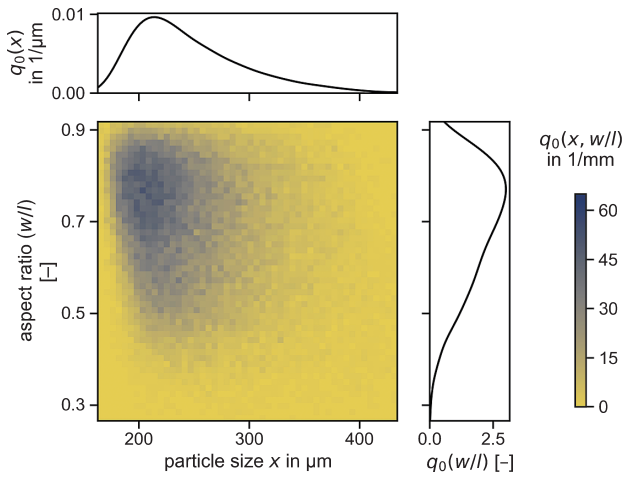

Fig. 11 Feed particle system discussed virtually separated in the model cases described in the text.

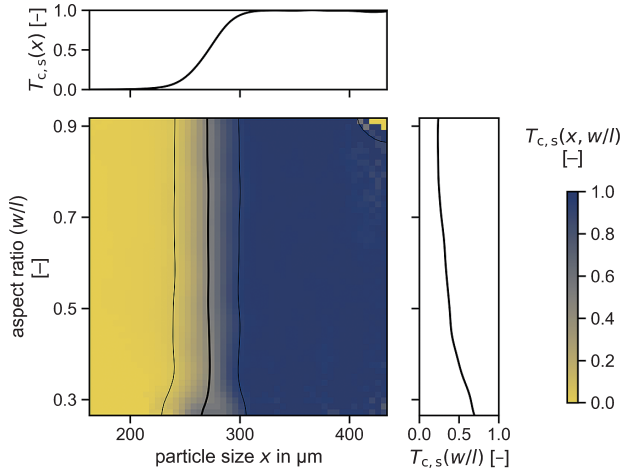

Fig. 12 Separation function for a one-dimensional separation according to size. The separation function is calculated from the probability distributions in **Figs. 11** and **12**. Isolines display a separation degree of 25 %, 50 %, and 75 %.

measures 2D projection areas of particles, this technique has the advantage of providing true volume and shape data for each particle.

The feed particle system (**Fig. 11**) shows a wide distribution of the particles in the definition range of size and shape. The distribution will be separated one- and multidimensionally.

4.4 Separation according to size

The separation according to size is virtually generated using a certain imperfection that leads to an interstitial regime and a certain spread of the separation function (**Fig. 12**). For the example given in **Fig. 13**, the marginal size fractions of concentrate and reject overlap in the size range between 200 µm and 300 µm.

The resulting separation function (**Fig. 12**) principally behaves like the model case for the separation according to size, showing a vertical slope. In addition to the median isoline, two further isolines are plotted, which represent the 25 % and 75 % values of the separation function. Looking at the marginal separation function, the function for size separation shows the known s-shaped form of a Tromp curve, whereas the function for shape separation in the real case is widely distributed and differs considerably from the ideal split behavior, which is due to a certain size dependency of the shape factor in the feed material.

4.5 Separation according to shape

The separation of the feed distribution according to shape generates a concentrate with higher aspect ratio and a reject with lower aspect ratio. The marginal distributions of the particle shape overlap for aspect ratios between 0.5 and 0.6. The marginal distributions in size appear to be quite similar (**Fig. 14**).

The resulting two-dimensional separation function (**Fig. 15**) shows a horizontal median isoline at an aspect ratio of approximately 0.55. The marginal separation

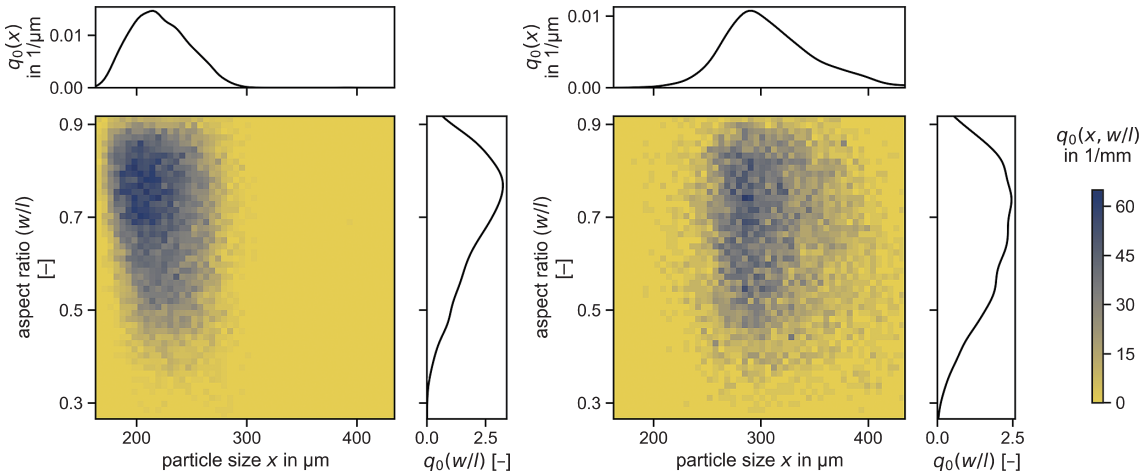

Fig. 13 Particle property distributions for the ideal separation according to particle size; **left**: reject; **right**: concentrate. The distributions sum to the feed displayed in **Fig. 10**.

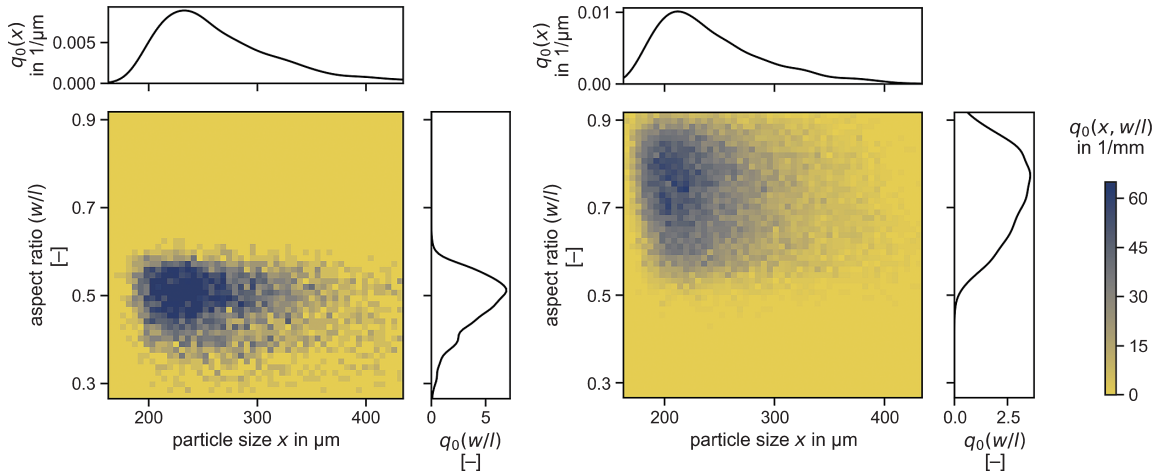

Fig. 14 Particle property distributions for the ideal separation according to particle shape; **left**: reject; **right**: concentrate. The distributions sum to the feed displayed in **Fig. 11**.

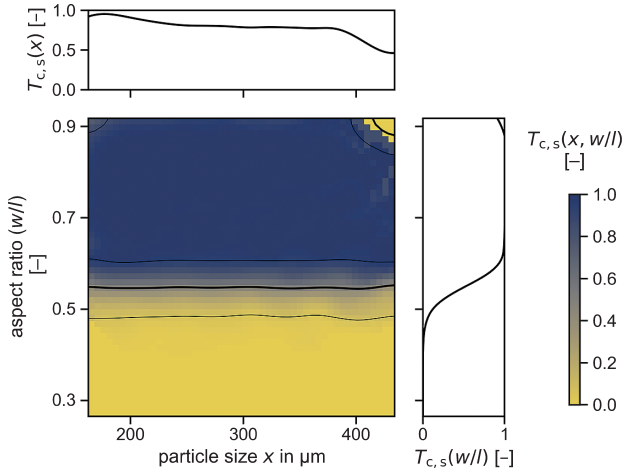

Fig. 15 Separation function for a separation according to particle shape, derived from the probability distributions of concentrate and feed in **Fig. 14** and **Fig. 11**, respectively. Isolines display a separation degree of 25 %, 50 %, and 75 %.

function for the aspect ratio shows the typical S-shape. The marginal separation function for the size separation has a quite high value of about 0.85 in the interval from 200 µm to 400 µm, indicating that only 15 % of the particles in this size class will end up in the reject. This result is due to the correlation between size and shape in the feed particle property distribution. In this size range, the size separation can be described as ideal split; however, above 400 µm the marginal separation function for size drops to below 0.5. In this size range the shape distribution of the particles changes and more particles will end up in the concentrate. The two-dimensional separation function also shows a second median isoline in the upper right corner, which is the two-dimensional analogion of the (one-dimensional) fishhook effect.

4.6 Two-step separation according to size and shape in series

In particle processing, the processing of a particle stream often involves several process steps in series to generate the required specifications of the particle system. When separation according to size and shape is performed in series, the final product, i.e., the concentrate, will contain all particles above a certain particle size and having an aspect ratio above a certain threshold (**Fig. 16, left**). The reject will contain all other particles.

The resulting separation function (**Fig. 17**) is the superposition of the two individual separation functions for the size and shape separation steps. The superposition generates a separation function that eliminates the upper right corner of the two-dimensional feed distribution. Due to this positioning of the two-dimensional function, the marginal separation functions appear to be quite imperfect. Both show an S-shaped increase near their individual threshold value, but this increase does not reach the value of 1, which is due to the fact that each particle has to fulfill two conditions to belong in the concentrate. Large particles with a small aspect ratio and small particles with high aspect ratio will therefore end up in the reject, making the one-dimensional separation functions never reach the value of 1.

4.7 Two-dimensional simultaneous separation according to size and shape

Most separation apparatuses will not separate particles according to a single feature. A real two-dimensional separation occurs when the combination of two or more features determines the separation result, i.e., when more than one properties become a separation feature in the separation process. The separation function can then have any geometrical appearance in the two- or multidimensional plot.

In the two-dimensional example, the concentrate

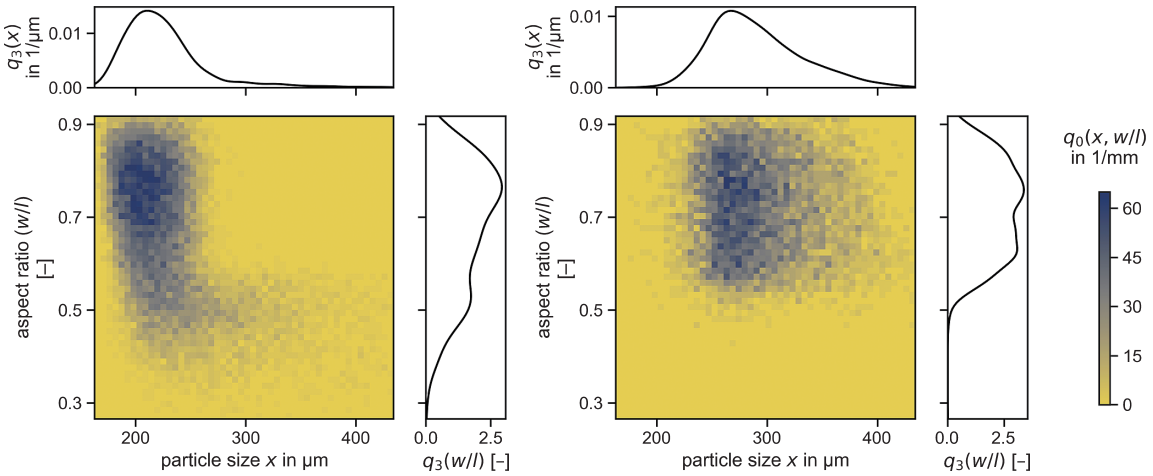

Fig. 16 Particle property distributions of concentrate **(left)** and reject **(right)** for a two-step separation according to size and shape, one after the other.

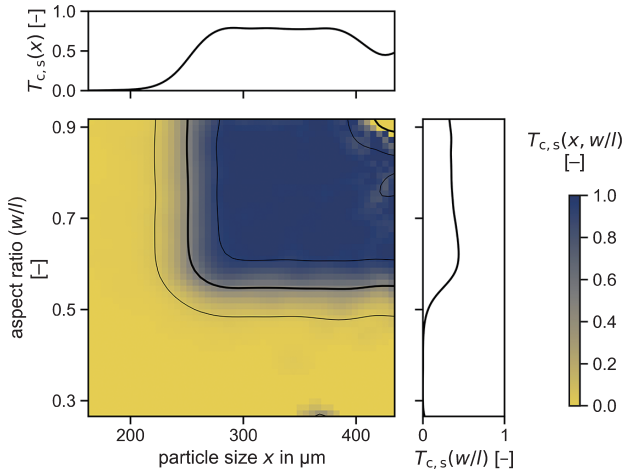

Fig. 17 Separation function of a two-step separation consisting of a first separation according to size and a second separation step according to shape, i.e., aspect ratio. Isolines display a separation degree of 25 %, 50 %, and 75 %.

contains larger particles with a higher aspect ratio (**Fig. 18**). The appearance of particles in the concentrate with a lower aspect ratio increases with increasing particle size.

The two-dimensional separation (**Fig. 19**) shows several effects. Firstly, because the median separation isoline has a certain slope, the two-dimensional function is influenced by both parameters: size and aspect ratio. Secondly, the distance between the isolines for the separation degrees of 25 %, 50 %, and 75 % is not constant; thus, the local sharpness of the separation is not constant within the definition range of the separation function.

The marginal separation function for particle size looks very much like a normal one-dimensional size separation. It is therefore not always apparent from one-dimensional separation functions, if there is an influence of another parameter. In contrast, the marginal separation function for aspect ratio looks very much nonideal, hinting at the effect of another parameter.

In the upper right corner of the diagram, the separation function decreases and does not have a value of 1. This can

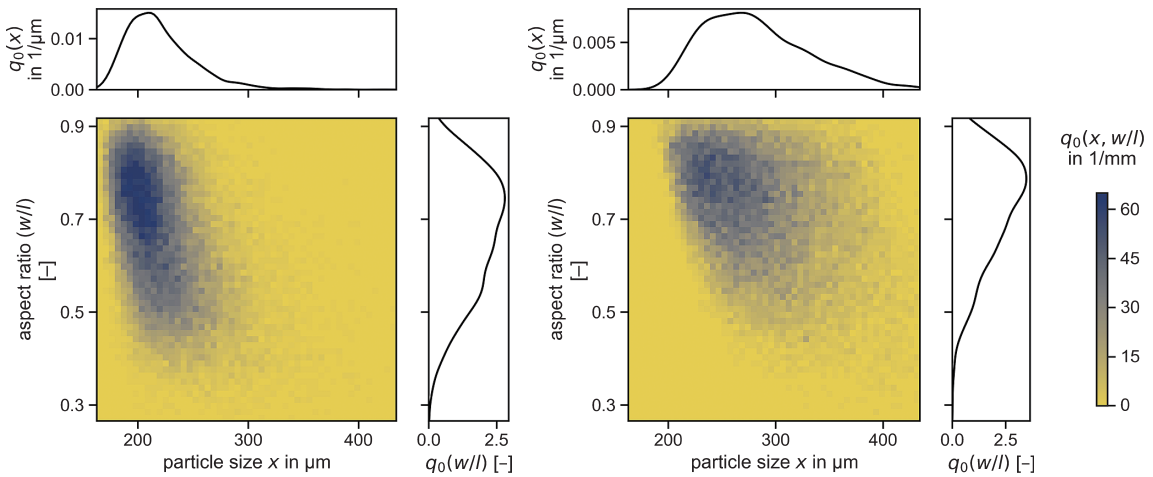

Fig. 18 Reject **(left)** and concentrate **(right)** fractions for a (single step) multidimensional separation that depends on both particle shape and size.

be a real property related to a decrease in the separation efficiency or an artifact, which derives from the fact that in that region the particle property distribution only contains a very small number of particles or does even contain no particles. The uncertainty of the separation function is also low in the lower right corner (large particle sizes and low aspect ratio), since that region does not contain many particles.

5. Application examples: two- and multi-dimensional separation

5.1 Analysis of the performance of an air classifier for lithium battery recycling

An air classifier, as described by Kaas A. et al. (2022), was used to separate different material fractions from the recycling process of lithium-ion batteries. The mechanical recycling route results in cathode and anode foils being separated from other material fractions like cell housing, wiring, and separator foil (Werner et al., 2022). The resulting fractions from the separation experiments were analyzed using an RGB-camera system and two-dimensional image analysis techniques. The air classifier in this step was supposed to generate at different gas velocities several material fractions out of the crushed battery cell, where besides the electrode coatings, aluminum and copper are the main valuable materials (Kaas et al., 2023).

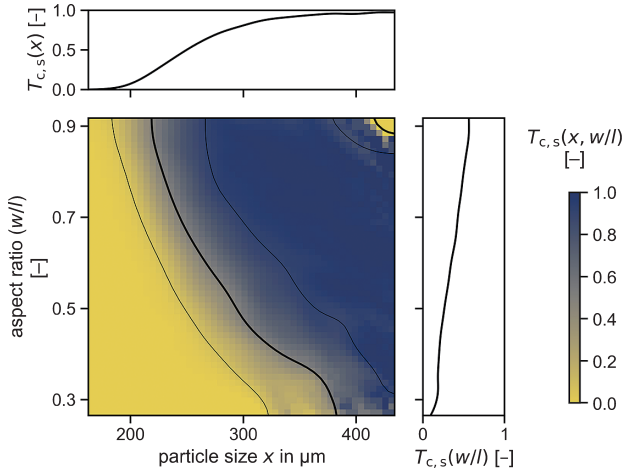

Fig. 19 Separation function for a single step two-dimensional separation, with both particle shape and particle size having an effect on the separation process.

Fig. 20 shows the resulting two-dimensional partition curves for particle size and shape, taking solely aluminum and copper or all fractions into account. From the first partition curve, aluminum results in the concentrate fraction within a specific variable area in the heat plot with relatively coarse, slightly compacted or platy particles. The smaller, more compacted particles are aluminum housing particles (**Fig. 20, left**). From the second partition curve (**Fig. 20, middle**), it can be seen that copper reports to the concentrate over a wide variable area of size and shape, including small compacted particles and coarse particles with low circularity. The last map (**Fig. 20, right**) shows the overall partition values weighted by the general particle area. It can be found that particles, in general, report to the concentrate at a particle size of > 40 mm and a circularity of < 0.6. In summary, the graphs show that separating shredded and compacted aluminum and copper foils as one of the main separation tasks in battery recycling can be successfully conducted using an air classifier. However, small copper particles with a low circularity are problematic, as they are recovered into the reject product stream. Actually, the dataset reflects a separation of a higher dimensionality than two-dimensional, since particle size, particle shape, and material composition are involved. To allow a consistent presentation of the results, no three-dimensional heat plots are used here.

5.2 Froth flotation

Froth flotation is a well-established and efficient processing technique for the separation of fine particle fractions. The method has gained attention in recycling applications recently (Vanderbruggen et al., 2021). It relies on the difference in particle wettability, i.e., hydrophobic particles attach to gas bubbles and are recovered in the froth, whereas hydrophilic particles remain suspended. Because of the complex interactions between the particles and the bubbles, further properties such as particle size, particle shape (Chen et al., 2022; Hassas et al., 2016; Koh

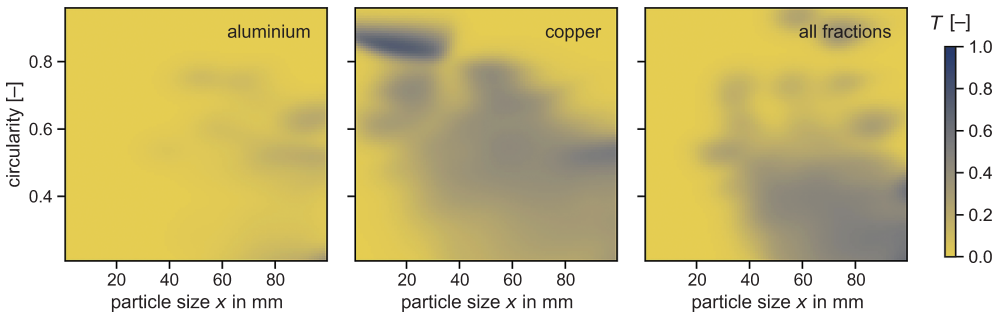

Fig. 20 Separation of crushed battery debris particles in a zig-zag air classifier; **left** separation function for aluminum; **middle** separation function for copper; **right** separation function for all materials.

et al., 2009; Verrelli et al., 2014; Wang et al., 2015; Xia, 2017), morphology, or composition affect the separation process as well. Therefore, generally speaking, the separation function of flotation is multidimensional. The size dependence of flotation is caused by inefficient particle attachment due to the lack of inertia for fine particles (approx. < 10 µm) and caused by high particle detachment rates for coarse particles (approx. −>200 µm). Although this size dependence can be found for all material systems, the optimal particle size for flotation depends on additional properties such as particle density (Farrokhpay et al., 2021; Hassanzadeh et al., 2022).

The modified flotation cell used in this study was designed specifically for the separation of particles below 10 µm. It combines the advantages of a mechanical flotation cell with a high particle-bubble collision rate (thus a high recovery) with those from a flotation column with a secondary fractionating effect due to its deep froth (thus a high grade). A schematic drawing of the newly designed *MultiDimFlot* cell is presented in **Fig. 21**, and more detailed information can be found in literature (Wilhelm et al., 2023).

To investigate the influence of specific particle properties on the separation process, tailored mixtures of particle fractions with defined properties are used to evaluate, e.g., the influence of particle shape and size on the separation efficiency in flotation. The mixture consists of either glass spheres or glass fragments as the floatable particle fraction mixed with magnetite as the non-floatable particle fraction. The wettability of the glass particles is modified via an esterification reaction with alcohols before flotation, thus resulting in glass particles with defined wettability states (C0—hydrophilic, C6—mildly hydrophobic, C10—strongly hydrophobic) (Sygusch and Rudolph, 2021).

Because of the detailed characterization of the separation products, which involves. XRF (X-ray fluorescence), SEM, and SEM–EDX, information on particle size, shape and composition is available.

The separation results are plotted for the different particle systems as two-dimensional heat plots, highlighting particle-equivalent diameter and aspect ratio as the main particle parameters, since these are available per particle, i.e., particle-discrete in **Fig. 22**. The further parameters, the surface energy, i.e., the wetting properties of the glass, and the predominant particle shape are investigated and presented as a parameter study. The multidimensional separation functions differ between the spherical and the irregular glass particles significantly. The definition range, where the separation function has the value of one, i.e., where the particles are transferred to the concentrate, is larger for the

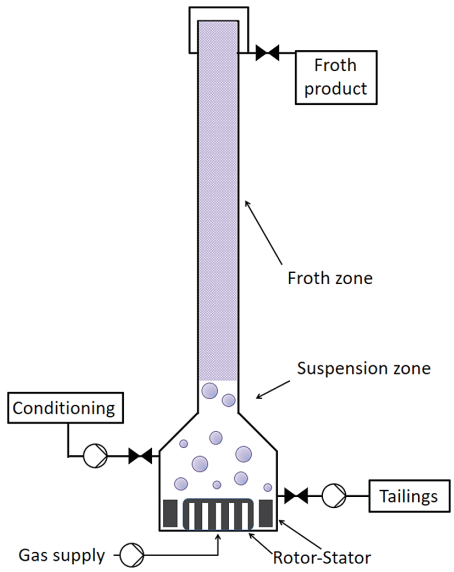

Fig. 21 Schematic drawing of the newly designed *MultiDimFlot* separation apparatus combining mechanical and column flotation. Adapted from Ref. (Sygusch et al., 2023) under the terms of the CC-BY 4.0 license. Copyright: (2023) The Authors, published by MDPI (Basel, Switzerland).

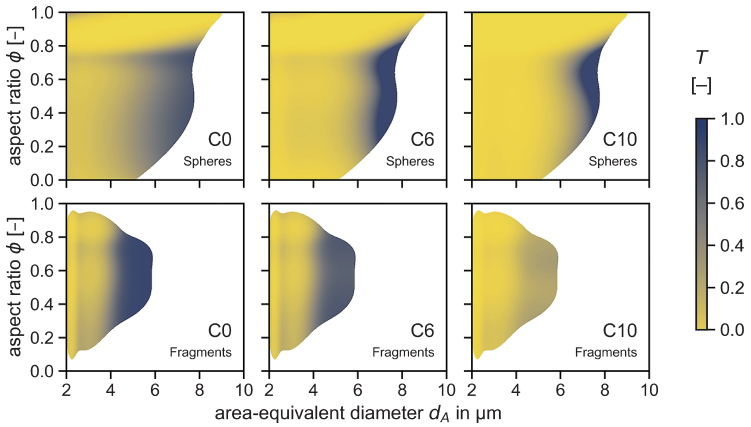

Fig. 22 Two-dimensional separation functions showing the combined influence of the shape (aspect ratio) and size (area-equivalent diameter) on the separation process; **upper row**: glass spheres and **lower row**: glass fragments. The hydrophobicity of the used glass particles increases from left to right (C0 = hydrophilic, C6 = mildly hydrophobic, C10 = strongly hydrophobic). Adapted from Ref. (Frank et al., 2023) under the terms of the CC-BY 4.0 license. Copyright: (2023) The Authors, published by MDPI (Basel, Switzerland).

predominant spherical shape of the feed (**Fig. 22**). The influence of the particle hydrophobicity is revealed when comparing separation functions of the same row, i.e spheres-C0 vs. spheres-C6 vs. spheres-C10, as the hydrophobicity of the glass particles increases from left to right in **Fig. 22**. It becomes visible that the sharpness of the separation increases along with the hydrophobicity of the spherical glass particles.

5.3 Beneficiation of a tin-bearing complex skarn ore

Recently, multiple research consortia have explored the extraction and beneficiation of the polymetallic Tellerhäuser deposit in Germany's Erzgebirge area (Werner and Axel, 2012). The deposit contains iron oxides, valuable sulfide minerals, and cassiterite, a crucial tin-bearing mineral that plays a significant role in its economic feasibility. Because of the high specific density of cassiterite (approx. 7 g/cm^3), gravity separation is one of the most critical processing steps in a possible beneficiation flowsheet, whereas the significant content of iron oxides in the ore is separated by magnetic separation. Gravity separation tests for ore samples obtained from the Tellerhäuser deposit were performed on a laboratory scale using a falcon density separator. In a pilot plant test with 140 t of material, a drum-type magnetic separator was used to produce a magnetic concentrate.

Furthermore, a shaking table was used to separate cassiterite from lighter mineral phases (Pereira et al., 2021). For all cases, including the falcon separator, the shaking table and the drum-type magnetic separator, samples of the products were investigated using MLA, allowing for particle-based analysis of the separation process by calculating two-dimensional distributions based on kernel density estimates. All three separation processes will be discussed in the following sections, showcasing the application of two-dimensional partition curves. The data for the processes described here are available online (Schach et al., 2021).

5.3.1 Magnetic separation in the pilot plant

In most magnetic separators, the electromagnetic characteristics of a particle collective are superposed by the particle mass (Oberteuffer, 1974; Oder, 1976; Svoboda and Fujita, 2003). Separation of the iron oxide phases is essential to achieve a high-quality cassiterite concentrate (Buchmann et al., 2018). The iron oxides present in the ore primarily consist of magnetite and hematite (Kern et al., 2019). Even though MLA can distinguish between magnetite and hematite using backscattered electron values (Figueroa et al., 2012), it cannot be employed in this study's ore because of fluctuations in BSE values caused by varying amounts of Sn and other elements in the crystal lattice (Kern et al., 2018). As a consequence of the inability to easily differentiate between the iron oxide phases, the magnetic susceptibility of the particles cannot be calculated, and the iron oxide content in the particles is used as a proxy for the separation property.

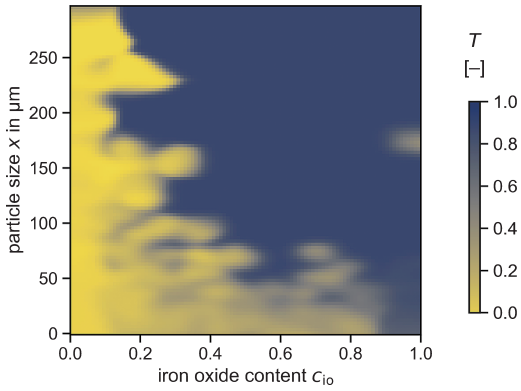

Fig. 23 Two-dimensional partition curve for the magnetic separation of a cassiterite ore.

A weak wet drum-type separator was installed in the pilot plant. The diameter of the drum was 900 mm at a drum width of 300 mm. During operation, the volume flow of the feed suspension was adjusted to 1.5 m^3/h with a solid content of 0.2 kg/m^3, and the drum speed was set to 18 rpm. The partition curve based on the MLA data is depicted in **Fig. 23**. The graph shows that coarse particles (> 150 µm) with an iron oxide content of more than 0.2–0.3 report to the magnetic concentrate. At smaller particle sizes, the threshold content of iron oxides within a particle to be recovered into the magnetic product increases. At particle sizes below 50 µm, the separation becomes unsharp even at high iron oxide contents of 0.6–0.8, which is indicated by *T*-values in the range of 0.4–0.6.

This behavior might be explained by fine hematite particles in the ore that do not respond to the drum-type separator's relatively low magnetic field density and gradient. Another explanation could be an inefficient extraction at such fine particle sizes due to agglomeration or slime-coating effects.

5.3.2 Gravity separation on a shaking table

Gravity separation technologies, with the exception of dense media separation, are fundamentally multidimensional separation processes, where the effects of density, particle size, and particle shape often influence the separation efficiency (Burt and Mills, 1984), since drag forces and field forces interact. Density separation in this example was realized using a shaking table that produced four streams: one product stream with a high content of liberated dense cassiterite, iron oxides, and arsenopyrite (Product 1), a product stream mainly comprising iron oxides but also significant amounts of cassiterite (Product 2), a middling stream containing intergrown cassiterite, and finally a tailing stream consisting of light mineral phases such as silicates.

The particles on the shaking table are separated by density and size along the width of the table, with small and heavy particles collected at one end of the separator followed by heavy-coarse particles and small-light particles contained in the middle of the shaking table. On the other end of the table, coarse-light particles are collected (Wills and Finch, 2016). The dimensions of the shaking table used in the pilot test is 3500 × 1500 mm. The volume flows of the feed suspension and the wash water were 0.3 m^3/h and 1.3 m^3/h, respectively, and the solid content of the feed suspension was 700 kg/m^3.

Fig. 24 shows a schematic of the used shaking table and the obtained streams. Based on MLA analysis, a mass-weighted distribution over particle density and particle size is plotted in **Fig. 25**. It is noteworthy that, especially prominent for the two product streams, the distribution shows distinct lines at certain density values representing the respective liberated mineral phases, e.g., cassiterite with a density of about 7 g/cm^3, iron oxides with a density of 4–5 g/cm^3, and arsenopyrite with a density of around 6 g/cm^3. Whereas product 1 mainly comprises particles below 100 µm with a significant concentration of cassiterite particles, product 2 mainly contains iron oxide particles in larger size fractions. For the feed, middling and tailing stream, particles are distributed over a wider size range at low particle densities indicating light mineral phases such as silicates.

For the calculation of the two-dimensional Tromp curve depicted in **Fig. 26**, product 1 was defined as concentrate stream and all other products were summarized as the reject. The graph shows that the shaking table has a cut point within the density range of 4–5 g/cm^3.

However, at particle sizes below 25 µm, particles have a high probability to be recovered in the tailing stream independent of their density. For particles within this size range, the shaking table is not able to effectively separate the minerals according to density and as a consequence fine cassiterite is lost in the reject in this application. Due to the brittle nature of cassiterite and its favorable enrichment in fine particle fractions, this behavior leads to unwanted losses of fine cassiterite.

5.4 Gravity separation in a Falcon separator

Gravity separation at laboratory scale with a Falcon Separator (Falcon L40 concentrator, **Fig. 27**) was used with 500 g ore samples as feed material and a water flow of 5 l/min. The riffled bowl of the separator rotated at a speed of 2300 rpm. Due to the resulting gravitational force, the heavy material was deposited in the riffles of the separator and scraped off at the end of the test. The light tailing material was discharged continuously.

The resulting partition curve (Schach et al., 2019) for the falcon separator is presented in **Fig. 28**. Both particle

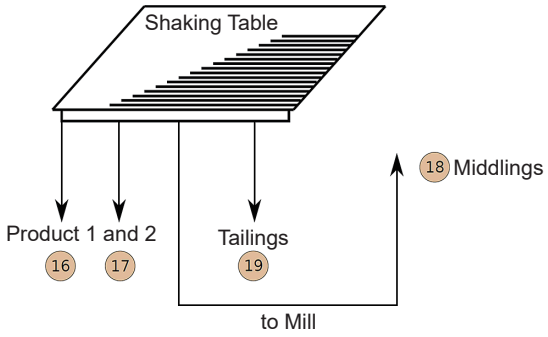

Fig. 24 Schematic of the shaking table with the respective product streams.

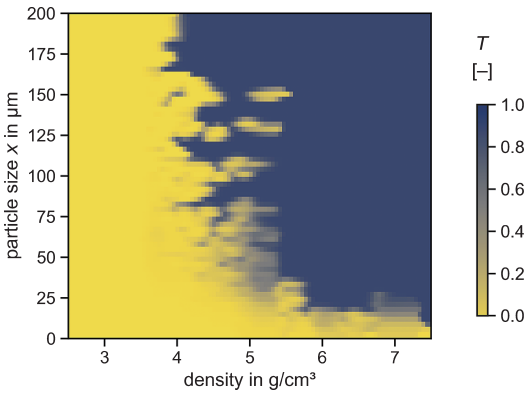

Fig. 26 Partition map for the shaking table over density and size defining product 1 as concentrate and the remaining streams as reject, tailing stream respectively.

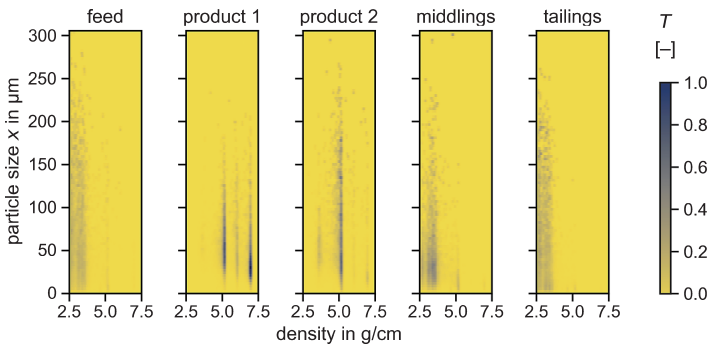

Fig. 25 Distributions for the feed and output streams of the shaking table over particle size and density.

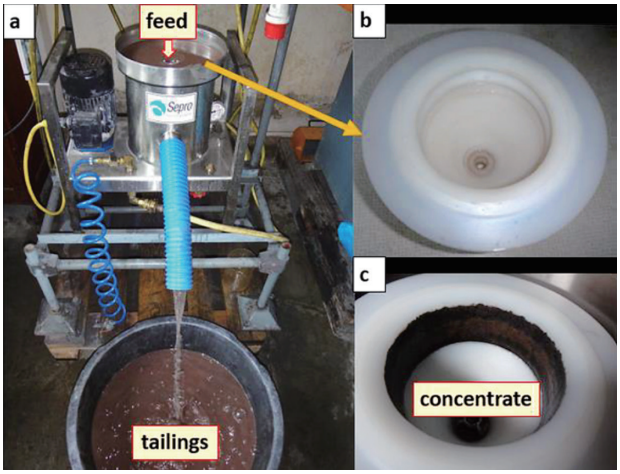

Fig. 27 Falcon separator: **(a)** experimental set up; **(b)** inner riffled bowl without material; **(c)** riffles filled with heavy material.

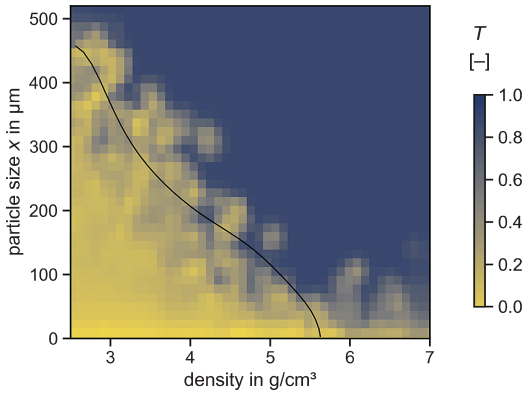

Fig. 28 Two-dimensional partition curve for the gravity separation via falcon concentrator. The line represents the cut function fitted to the points with a partition value of 50 %, displayed as points in the graph. Adapted with permission from Ref. (Schach et al., 2019). Copyright: (2019) Elsevier B.V.

properties—density and size—influence the partition of particles (Rao et al., 2003). It can be concluded that the separation process is rather dependent on the particle mass, resulting in higher inertia during separation, than solely on particle density or particle size (Nayak et al., 2021). Below a particle size in the range of 20–30 µm, the partition remains low for all density values. In this size range, the separation device cannot effectively separate cassiterite from the light minerals due to, e.g., slime coating of the fine cassiterite particles on coarser silica particles. Here, the drag forces determine the movement of all particles.

5.5 Aerodynamic lens

A classifying aerodynamic lens can be used to fractionate aerosols by particle size and particle density at the same time (Kiesler et al., 2019; Wang et al., 2005a, 2005b). The window of application of such a separation system depends on the flow regime and the geometry of the lens itself and is located in the upper nm range. The operation parameters

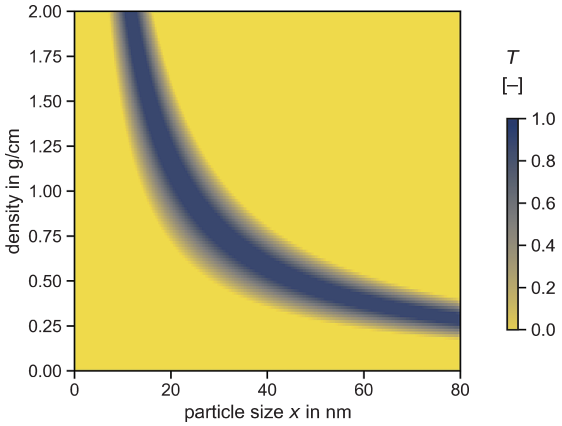

Fig. 29 Two-dimensional separation function of an aerodynamic lens. Adapted with permission from Ref. (Furat et al., 2020). Copyright: (2020) Elsevier B.V.

allow the tailoring of the separation function, i.e., the product received as concentrate.

Classifying aerodynamic lenses are orifices that constrict aerosol flow through a radially symmetric pipe. If the flow is laminar, and the starting position of a particle upstream of the lens is known, the end position downstream of the lens is a function of its specific relaxation time. Therefore, the feed is injected at a defined central position. The relaxation time is a function of different parameters, such as the pressure upstream of the lens, the flow rate through the lens, and the lens diameter, and it further depends on the particle properties, e.g., the particle size, shape, and density. In the setup discussed in Furat et al. (2020), the aerosol particles are injected into a laminar sheath gas flow at an off-axis position. Extracting aerosol downstream of the lens at a central position gives the separating aerodynamic lens a differential transfer characteristic, where only particles within a small range of particle properties such as size and solid density are collected. This becomes clearly visible in the two-dimensional plot for the separation function (**Fig. 29**), which has only a small and defined area of particle properties, where the separation function is one.

5.6 Hydrocyclone

The two-dimensional separation for plate-shaped particles having different aspect ratios has been discussed by Frank et al. for a hydrocyclone (Frank et al., 2023). The particle shape is assumed to be a flat regular cylinder with diameter d and thickness l. The separation efficiency presented uses a theoretical model that contains the shape dependency by taking its dependency on the drag force into account. The separation function (**Fig. 30**) based on this model shows over a long range of the thickness l of the plates only a dependence on the particle diameter d, resulting in a vertical isoline similar to the discussion of the respective ideal one-dimensional case in **Fig. 9**. The separation becomes two-dimensional with decreasing

particle thickness. Below about 1 µm there is a significant dependency of the separation function on both parameters: diameter and plate thickness, which is indicated by a deviation of the isoline from the ideal behavior of the one-dimensional case. Nevertheless, it can be stated that the hydrocyclone described by this model is predominantly a classification apparatus with only small capacities in two- or multidimensional separation. The effect of particle shape on the separation is not pronounced for the range of particle dimensions investigated. This might change for coarser particles. Real experiments to validate this model approach are still lacking.

5.7 Disc-stack centrifuge

Applying theoretical models for the separation efficiency by sedimentation, Frank et al. generated a two-dimensional separation function for a disc-stack centrifuge (**Fig. 31**) (Frank et al., 2023). As it is fundamentally known that the sedimentation velocity depends on the particle-equivalent diameter to the square as well as to the particle density difference between carrier media and solids, the multidimensional separation probability can be plotted using these two influencing parameters. The results show a slight negative slope of the 50 % isoline in the separation function, which states that separation by size is the predominant effect and there is only a smaller influence of the particle density in this machine. Thus, the sedimentation in the disc-stack centrifuge still is a classification process with a certain contribution of the effect of equal settling velocity for small dense and large light particles.

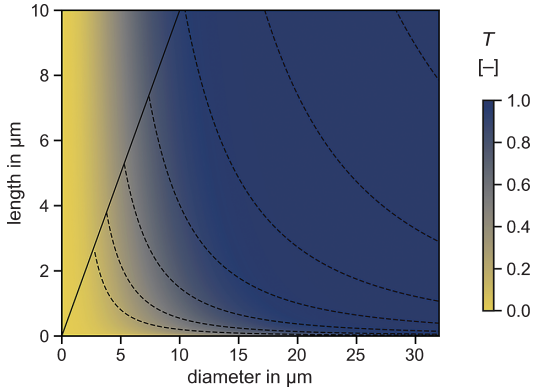

Fig. 30 Theoretically deducted two-dimensional separation function for the separation of plate shaped cylindrical particles in a hydrocyclone. Adapted from Ref. (Frank et al., 2023) under the terms of the CC-BY 4.0 license. Copyright: (2023) The Authors, published by MDPI (Basel, Switzerland).

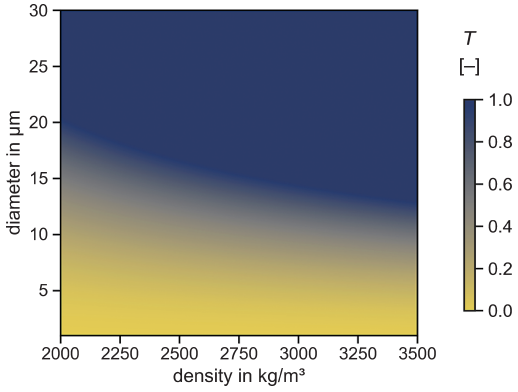

Fig. 31 Theoretically deducted two-dimensional separation function for the separation of model particles being distributed in size and density in a disk-stack centrifuge. Adapted from Ref. (Frank et al., 2023) under the terms of the CC-BY 4.0 license. Copyright: (2023) The Authors, published by MDPI (Basel, Switzerland).

5.8 High-gradient magnetic separation

Three commercially available, rare-earth-doped lamp phosphor particle collectives obtained from Leuchtstoffwerk Breitungen GmbH (Breitungen, Germany) were used. These included a cerium/terbium-doped lanthanum phosphate ($LaPO_4$:Ce^{3+}, Tb^{3+}, LAP), a europium-doped barium magnesium aluminate ($BaMgAl_{10}O_{17}$:Eu^{2+}, BAM), and a europium-doped yttrium oxide (Y_2O_3:Eu^{3+}, YOX). Due to their rare earth content, the particles exhibit paramagnetic properties, with LAP having the highest magnetic susceptibility at 3.69×10^{-3}, followed by BAM at 1.19×10^{-3} and YOX at 0.516×10^{-3}. Their use as illuminants and the associated fluorescence of the compounds allowed for quantitative analysis through fluorimetry.

For conducting fractionation experiments of the particle mixture, a fast protein liquid chromatography (FPLC) system (ÄKTA purifier, Cytiva, Buckinghamshire, UK) equipped with polyetheretherketone (PEEK) tubing was employed. The schematic flow diagram in **Fig. 32** illustrates the process of magnetic field-controlled chromatography. A defined mixture of low salt (1a) and high salt (1b) buffer was pumped into the system, mixed (2), and injection pulses ($V = 0.5$ mL) were introduced to the fluid stream through an injection loop and valve (3). The mobile phase, along with the injected particle suspension, flowed onto the column, which was surrounded by an external magnetic field source (4) connected to a power supply (5). The effluent was then collected and separated into distinct

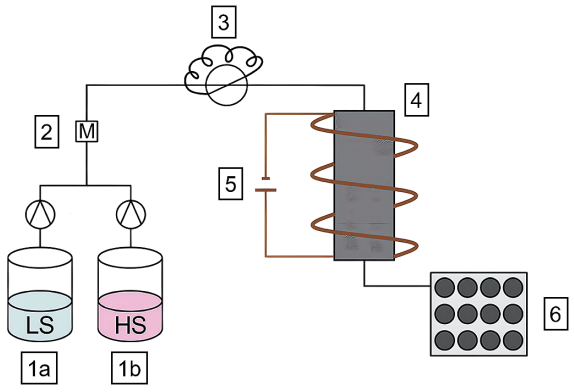

Fig. 32 General flow diagram for the fractionation experiment.

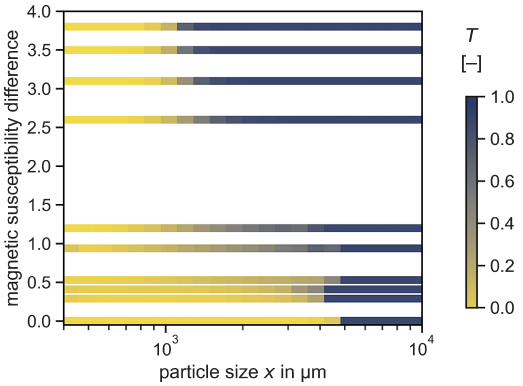

Fig. 33 The separation function for magnetic chromatography retrieved from different particle systems consisting of distinct materials with distinct magnetic properties.

fractions at the outlet of the column using a fraction collector (6). Continuous monitoring of the process was performed using an in-line UV/VIS cell at 280 nm.

The magnetic force induced between the paramagnetic particles and the magnetized chromatography matrix elements is influenced by the particle size as well as the intrinsic magnetic susceptibilities of the particles and the magnetic susceptibility of the surrounding fluid. Consequently, when the susceptibility difference between the dispersed and continuous phases decreases, the magnitude of the magnetic force diminishes. Therefore, by dissolving paramagnetic salts such as manganese(II)-chloride in the continuous phase and employing various particle types with distinct magnetic susceptibilities, which prevent a continuous display of the two-dimensional degree of separation (see **Fig. 33**), it is possible to deliberately adjust the magnetic susceptibility difference. However, the solubility of the salt in the solution constrains this approach. In theory, by maintaining constant process parameters (such as flow rate and magnetic flux intensity), the size fractionation result can be altered by adjusting the salt concentration in the buffer.

6. Conclusions

Particle separation processes are, in most cases, influenced by multiple particle properties such as size, shape, and composition. However, the conventional one-dimensional separation function or Tromp curve fails to capture the multidimensional distribution of particles and their effect on separation. Therefore, it's crucial to account for and define the Tromp curve for the multidimensional space. Knowing the multidimensional property distribution of feed, concentrate, and reject, it is possible to define and express the multidimensional separation function in a formal manner. This separation function has the same dimensionality as the property distributions of the related material streams. Furthermore, it is possible to define characteristic values for a multidimensional property distribution, like the median particle size (x_{50}, y_{50}) and a median isoline, where the value of the separation function equals $T(x, y) = 0.5$. Several application examples and the discussion of model cases of the two-dimensional separation function show that multidimensional separation occurs in many applications and that it can be described, quantified, and discussed using the methods shown.

Acknowledgements

This scientific work was mainly financed from projects within the Priority Programme 2045 of the German Science Foundation (DFG), with the project No. 313858373. Some scientific results stem as well from the projects DIGISORT (No. 03XP0337A) and AFK (No. 033R128) funded by the German Ministry for Education and Research (BMBF).

Nomenclature

A	area of plot (pixel^2)
C	index for concentrate (-)
c	mass fraction of concentrate (kg/kg)
c_{io}	iron oxide content (kg/kg)
d_A	area-equivalent diameter (m)
i	class index for first parameter (x) (-)
j	class index for second parameter (y) (-)
m	mass (kg)
m_i	mass of particle class i (kg)
q_r	density distribution weighted by quantity of dimension r (variable)
q_3	volume-/mass-based density distribution (variable)
q_{res}	sum of density distributions, distribution of mixture (variable)
Q_3	volume-/mass-based cumulative sum function (-)
$\Delta Q_{3,i,j}$	volume-/mass-based fraction of particles in a two-dimensional distribution (-)
R	index for retentate (-)
r	mass fraction of retentate (kg/kg)
S	index for supply, feed (-)
T	separation function, partition value (-)
x	particle size (equivalent diameter) (m)
x_i	upper particle size of a given class (m)
$\overline{x_i}$	average particle size of a given class (m)
Δx_i	particle size interval of a given class (m)
x_{min}	minimum particle size of a distribution (m)
x_{max}	maximum particle size of a distribution (m)
y	second parameter, e.g., shape factor (variable)
μ	integrating index for first parameter (x) (-)
ν	mass fraction (kg/kg), integrating index for second parameter (y) (-)

References

Alonso M., Satoh M., Miyanami K., Mechanism of the combined coating-mechanofusion processing of powders, Powder Technology, 59 (1989) 45–52. https://doi.org/10.1016/0032-5910(89)80094-4

Baalousha M., Stolpe B., Lead J.R., Flow field-flow fractionation for the analysis and characterization of natural colloids and manufactured nanoparticles in environmental systems: a critical review, Journal of Chromatography A, 1218 (2011) 4078–4103. https://doi.org/10.1016/j.chroma.2011.04.063

Bagheri G.H., Bonadonna C., Manzella I., Vonlanthen P., On the characterization of size and shape of irregular particles, Powder Technology, 270 (2015) 141–153.

https://doi.org/10.1016/j.powtec.2014.10.015
Baloun T.A., Schoenherr J.I., Zocher M., Schubert G., Studies on thermoadhesion-based sorting, Aufbereitungstechnik, 46 (2005) 12–27.
Blott S.J., Pye K., Particle shape: a review and new methods of characterization and classification, Sedimentology, 55 (2008) 31–63. https://doi.org/10.1111/j.1365-3091.2007.00892.x
Bourgeois F., Majumder A.K., Is the fish-hook effect in hydrocyclones a real phenomenon?, Powder Technology, 237 (2013) 367–375. https://doi.org/10.1016/j.powtec.2012.12.017
Buchmann M., Schach E., Leißner T., Kern M., Mütze T., Rudolph M., Peuker U.A., Tolosana-Delgado R., Multidimensional characterization of separation processes – Part 2: comparability of separation efficiency, Minerals Engineering, 150 (2020a) 106284. https://doi.org/10.1016/j.mineng.2020.106284
Buchmann M., Schach E., Rudolph M., Peuker U., Boogaart G., Tolosana-Delgado R., Multidimensional particle-based process characterization, Proceedings of the IMPC (International Mineral Processing Congress), 2020b, pp10.
Buchmann M., Schach E., Tolosana-Delgado R., Leißner T., Astoveza J., Kern M., Möckel R., Ebert D., Rudolph M., van den Boogaart K., Peuker U., Evaluation of magnetic separation efficiency on a cassiterite-bearing skarn ore by means of integrative SEM-based image and XRF–XRD data analysis, Minerals, 8 (2018) 390. https://doi.org/10.3390/min8090390
Buchwald T., Ditscherlein R., Peuker U.A., Beschreibung von Trennoperationen mit mehrdimensionalen Partikeleigenschaftsverteilungen, Chemie Ingenieur Technik, 95 (2023) 199–209. https://doi.org/10.1002/cite.202200109
Bujak B., Bottlinger M., Three-dimensional measurement of particle shape, Particle & Particle Systems Characterization, 25 (2008) 293–297. https://doi.org/10.1002/ppsc.200800027
Burt R.O., Mills C., Gravity Concentration Technology, Elsevier, 1984, ISBN: 9780444424112.
Chen Y., Zhuang L., Zhang Z., Effect of particle shape on particle-bubble interaction behavior: a computational study using discrete element method, Colloids and Surfaces A: Physicochemical and Engineering Aspects, 653 (2022) 130003. https://doi.org/10.1016/j.colsurfa.2022.130003
Çiçek Ö., Abdulkadir A., Lienkamp S.S., Brox T., Ronneberger O., 3D U-Net: learning dense volumetric segmentation from sparse annotation, Medical Image Computing and Computer-Assisted Intervention – MICCAI 2016, Cham, Springer International Publishing, (2016). https://doi.org/10.1007/978-3-319-46723-8_49
Czado C., Analyzing Dependent Data with Vine Copulas, Springer International Publishing, 2019, ISBN: 9783030137847.
Dehghani A., Monhemius A.J., Gochin R.J., Evaluating the Nakajima et al. model for rectangular-aperture screens, Minerals Engineering, 15 (2002) 1089–1094. https://doi.org/10.1016/s0892-6875(02)00225-x
Demeler B., Nguyen T.-L., Gorbet G.E., Schirf V., Brookes E.H., Mulvaney P., El-Ballouli A.a.O., Pan J., Bakr O.M., Demeler A.K., Uribe B.I.H., Bhattarai N., Whetten R.L., Characterization of size, anisotropy, and density heterogeneity of nanoparticles by sedimentation velocity, Analytical Chemistry, 86 (2014) 7688–7695. https://doi.org/10.1021/ac501722r
Ditscherlein R., Furat O., de Langlard M., de Souza e Silva J.M., Sygusch J., Rudolph M., Leißner T., Schmidt V., Peuker U.A., Multiscale tomographic analysis for micron-sized particulate samples, Microscopy and Microanalysis, 26 (2020) 676–688. https://doi.org/10.1017/s1431927620001737
Egan C.K., Jacques S.D.M., Wilson M.D., Veale M.C., Seller P., Beale A.M., Pattrick R.A.D., Withers P.J., Cernik R.J., 3D chemical imaging in the laboratory by hyperspectral X-ray computed tomography, Scientific Reports, 5 (2015) 15979. https://doi.org/10.1038/srep15979
Farrokhpay S., Filippov L., Fornasiero D., Flotation of fine particles: a review, Mineral Processing and Extractive Metallurgy Review, 42 (2021) 473–483. https://doi.org/10.1080/08827508.2020.1793140
Figueroa G., Moeller K., Buhot M., Gloy G., Haberla D., Advanced discrimination of hematite and magnetite by automated mineralogy, Proceedings of the 10th International Congress for Applied Mineralogy (ICAM), Berlin, Heidelberg, Springer Berlin Heidelberg, (2012).
Fontein F.J., Wirkung des hydrozyklons und des bogensiebs sowie deren anwendungen, Aufbereitungs-Technik, 2 (1961) 85–89.
Frank U., Dienstbier J., Tischer F., Wawra S.E., Gromotka L., Walter J., Liers F., Peukert W., Multidimensional fractionation of particles, Separations, 10 (2023) 252. https://doi.org/10.3390/separations10040252
Frank U., Uttinger M.J., Wawra S.E., Lübbert C., Peukert W., Progress in multidimensional particle characterization, KONA Powder and Particle Journal, 39 (2022) 3–28. https://doi.org/10.14356/kona.2022005
Frank U., Wawra S.E., Pflug L., Peukert W., Multidimensional particle size distributions and their application to nonspherical particle systems in two dimensions, Particle & Particle Systems Characterization, 36 (2019) 1800554. https://doi.org/10.1002/ppsc.201800554
Friebel J.M., Ditscherlein R., Ditscherlein L., Peuker U.A., Three-dimensional characterization of dry particle coating structures originating from the mechano-fusion process, Microscopy and Microanalysis, 30 (2024) 179–191. https://doi.org/10.1093/mam/ozae009
Friedländer T., Kuyumcu H.Z., Rolf L., Investigations into sorting PET flakes by particle shape, Aufbereitungstechnik, 47 (2006) 24–35.
Furat O., Leißner T., Bachmann K., Gutzmer J., Peuker U., Schmidt V., Stochastic modeling of multidimensional particle properties using parametric copulas, Microscopy and Microanalysis, 25 (2019) 720–734. https://doi.org/10.1017/s1431927619000321
Furat O., Masuhr M., Kruis F.E., Schmidt V., Stochastic modeling of classifying aerodynamic lenses for separation of airborne particles by material and size, Advanced Powder Technology, 31 (2020) 2215–2226. https://doi.org/10.1016/j.apt.2020.03.014
Furchner B., Zampini S., Air classifying, in: Wiley-VCH (Ed.), Ullmann's Ecyclopedia of Industrial Chemistry, Wiley-VCH Verlag GmbH & Co. KGaA, Weinheim, 2009, ISBN: 9783527306732. https://doi.org/10.1002/14356007.b02_17.pub2
Furuuchi M., Gotoh K., Shape separation of particles, Powder Technology, 73 (1992) 1–9. https://doi.org/10.1016/0032-5910(92)87001-Q
Hassanzadeh A., Safari M., Hoang D.H., Khoshdast H., Albijanic B., Kowalczuk P.B., Technological assessments on recent developments in fine and coarse particle flotation systems, Minerals Engineering, 180 (2022) 107509. https://doi.org/10.1016/j.mineng.2022.107509
Hassas B.V., Caliskan H., Guven O., Karakas F., Cinar M., Celik M.S., Effect of roughness and shape factor on flotation characteristics of glass beads, Colloids and Surfaces A: Physicochemical and Engineering Aspects, 492 (2016) 88–99. https://doi.org/10.1016/j.colsurfa.2015.12.025
Heywood H., Techniques for the evaluation of powders. i. fundamental properties of particles and methods of sizing analysis, Powder Metallurgy, 4 (1961) 1–28. https://doi.org/10.1179/pom.1961.4.7.001
Hickstein B., Peuker U.A., Modular process for the flexible synthesis of magnetic beads—Process and product validation, Journal of Applied Polymer Science, 112 (2009) 2366–2373. https://doi.org/10.1002/app.29655
Joe H., Dependence Modeling with Copulas, 1st edition, Taylor & Francis Group, 2014, ISBN: 9780429103186. https://doi.org/10.1201/b17116
Kaas A., Mütze T., Peuker U.A., Review on Zigzag Air Classifier, Processes, 10 (2022) 764. https://doi.org/10.3390/pr10040764
Kaas A., Wilke C., Vanderbruggen A., Peuker U.A., Influence of different discharge levels on the mechanical recycling efficiency of lithium-ion batteries, Waste Management, 172 (2023) 1–10. https://doi.org/10.1016/j.wasman.2023.08.042
Kern M., Kästner J., Tolosana-Delgado R., Jeske T., Gutzmer J., The inherent link between ore formation and geometallurgy as documented by complex tin mineralization at the Hämmerlein deposit (Erzgebirge, Germany), Mineralium Deposita, 54 (2019) 683–698. https://doi.org/10.1007/s00126-018-0832-2
Kern M., Möckel R., Krause J., Teichmann J., Gutzmer J., Calculating the deportment of a fine-grained and compositionally complex Sn skarn with a modified approach for automated mineralogy, Minerals

Engineering, 116 (2018) 213–225. https://doi.org/10.1016/j.mineng.2017.06.006

Kiesler D., Bastuck T., Kennedy M.K., Kruis F.E., Development of a high flow rate aerodynamic lens system for inclusion of nanoparticles into growing PVD films to form nanocomposite thin films, Aerosol Science and Technology, 53 (2019) 630–646. https://doi.org/10.1080/02786826.2019.1587149

Koh P.T.L., Hao F.P., Smith L.K., Chau T.T., Bruckard W.J., The effect of particle shape and hydrophobicity in flotation, International Journal of Mineral Processing, 93 (2009) 128–134. https://doi.org/10.1016/j.minpro.2009.07.007

Kuzmanić T., Mikoš M., Effect of coarse gravel and cobble size particles shape on their dynamic image analysis results, EGU General Assembly 2022, (2022) EGU22-4865. https://doi.org/10.5194/egusphere-egu22-4865

Lamberg P., Vianna S., A Technique for Tracking Multiphase Mineral Particles in Flotation Circuits, XXII ENTMME / VII MSHMT, (2007) pp9.

Leißner T., Bachmann K., Gutzmer J., Peuker U.A., MLA-based partition curves for magnetic separation, Minerals Engineering, 94 (2016) 94–103. https://doi.org/10.1016/j.mineng.2016.05.015

Leißner T., Diener A., Löwer E., Ditscherlein R., Krüger K., Kwade A., Peuker U.A., 3D ex-situ and in-situ X-ray CT process studies in particle technology – A perspective, Advanced Powder Technology, 31 (2020) 78–86. https://doi.org/10.1016/j.apt.2019.09.038

Matsuyama T., Yamamoto H., Particle shape and laser diffraction: a discussion of the particle shape problem, Journal of Dispersion Science and Technology, 25 (2005) 409–416. https://doi.org/10.1081/dis-200025692

Nageswararao K., A critical analysis of the fish hook effect in hydrocyclone classifiers, Chemical Engineering Journal, 80 (2000) 251–256. https://doi.org/10.1016/S1383-5866(00)00098-8

Nakajima Y., Whiten W.J., White M.E., Behaviour of non-spherical particles in screening, Transactions of Institution of Mining and Metallurgy, 88 (1979) C88–92.

Nayak A., Jena M.S., Mandre N.R., Application of enhanced gravity separators for fine particle processing: an overview, Journal of Sustainable Metallurgy, 7 (2021) 315–339. https://doi.org/10.1007/s40831-021-00343-5

Oberteuffer J., Magnetic separation: a review of principles, devices, and applications, IEEE Transactions on Magnetics, 10 (1974) 223–238. https://doi.org/10.1109/tmag.1974.1058315

Oder R., High gradient magnetic separation theory and applications, IEEE Transactions on Magnetics, 12 (1976) 428–435. https://doi.org/10.1109/tmag.1976.1059076

Oliver M., Matúš Č., Ľudmila G., Martin J., Radovan R., Peter P., Dynamic image analysis to determine granule size and shape, for selected high shear granulation process parameters, Strojnícky časopis - Journal of Mechanical Engineering, 69 (2019) 57–64. https://doi.org/10.2478/scjme-2019-0043

Peciar P., Jezso K., Kohutova M., GustafÃ-k A., Kratky L., Fekete R., Jirout T., Peciar M., Particle size distribution analysis of beech chips depending on the measurement method, Chemical Engineering Transactions, 92 (2022) 43–48. https://doi.org/10.3303/CET2292008

Pereira L., Frenzel M., Khodadadzadeh M., Tolosana-Delgado R., Gutzmer J., A self-adaptive particle-tracking method for minerals processing, Journal of Cleaner Production, 279 (2021) 123711. https://doi.org/10.1016/j.jclepro.2020.123711

Pfeffer R., Dave R.N., Wei D., Ramlakhan M., Synthesis of engineered particulates with tailored properties using dry particle coating, Powder Technology, 117 (2001) 40–67. https://doi.org/10.1016/s0032-5910(01)00314-x

Rao B.V., Kapur P.C., Konnur R., Modeling the size–density partition surface of dense-medium separators, International Journal of Mineral Processing, 72 (2003) 443–453. https://doi.org/10.1016/s0301-7516(03)00118-2

Schach E., Buchmann M., Tolosana-Delgado R., Leißner T., Kern M., van den Boogaart K.G., Rudolph M., Peuker U.A., Multidimensional characterization of separation processes – Part 1: introducing kernel methods and entropy in the context of mineral processing using SEM-based image analysis, Minerals Engineering, 137 (2019) 78–86. https://doi.org/10.1016/j.mineng.2019.03.026

Schach E., Padula F., Buchmann M., Möckel R., Ebert D., Pereira L., Kern M., Leißner T., Pashkevich D., Sousa R., Bremerstein I., Breuer B., Oliver K., Seltmann R., …van den Boogaart K.G., Data from a pilot plant experiment for the processing of a complex tin skarn ore - 19.11.2018, Dataset, Rodare, 2021. https://doi.org/10.14278/rodare.715

Svoboda J., Fujita T., Recent developments in magnetic methods of material separation, Minerals Engineering, 16 (2003) 785–792. https://doi.org/10.1016/s0892-6875(03)00212-7

Sygusch J., Rudolph M., A contribution to wettability and wetting characterisation of ultrafine particles with varying shape and degree of hydrophobization, Applied Surface Science, 566 (2021) 150725. https://doi.org/10.1016/j.apsusc.2021.150725

Sygusch J., Stefenelli N., Rudolph M., Ultrafine particle flotation in a concept flotation cell combining turbulent mixing zone and deep froth fractionation with a special focus on the property vector of particles, Minerals, 13 (2023) 1099. https://doi.org/10.3390/min13081099

Tang P., Puri V.M., Segregation quantification of two-component particulate mixtures: effect of particle size, density, shape, and surface texture, Particulate Science and Technology, 25 (2007) 571–588. https://doi.org/10.1080/02726350701783977

Tanno K., Current status of the mechanofusion process for producing composite particles, KONA Powder and Particle Journal, 8 (1990) 74–82. https://doi.org/10.14356/kona.1990014

Vanderbruggen A., Sygusch J., Rudolph M., Serna-Guerrero R., A contribution to understanding the flotation behavior of lithium metal oxides and spheroidized graphite for lithium-ion battery recycling, Colloids and Surfaces A: Physicochemical and Engineering Aspects, 626 (2021) 127111. https://doi.org/10.1016/j.colsurfa.2021.127111

Verrelli D.I., Bruckard W.J., Koh P.T.L., Schwarz M.P., Follink B., Particle shape effects in flotation. Part 1: microscale experimental observations, Minerals Engineering, 58 (2014) 80–89. https://doi.org/10.1016/j.mineng.2014.01.004

Wadell H., Sedimentation and sedimentology, Science, 75 (1932a) 20. https://doi.org/10.1126/science.75.1931.20.a

Wadell H., Volume, shape, and roundness of rock particles, The Journal of Geology, 40 (1932b) 443–451.

Wadell H., Sphericity and roundness of rock particles, The Journal of Geology, 41 (1933) 310–331. https://doi.org/10.1086/624040

Wang L., Peng Y., Runge K., Bradshaw D., A review of entrainment: mechanisms, contributing factors and modelling in flotation, Minerals Engineering, 70 (2015) 77–91. https://doi.org/10.1016/j.mineng.2014.09.003

Wang X., Gidwani A., Girshick S.L., McMurry P.H., Aerodynamic focusing of nanoparticles: ii. numerical simulation of particle motion through aerodynamic lenses, Aerosol Science and Technology, 39 (2005a) 624–636. https://doi.org/10.1080/02786820500181950

Wang X., Kruis F.E., McMurry P.H., Aerodynamic focusing of nanoparticles: i. guidelines for designing aerodynamic lenses for nanoparticles, Aerosol Science and Technology, 39 (2005b) 611–623. https://doi.org/10.1080/02786820500181901

Werner D., Peuker U.A., Mütze T., Recycling chain for spent lithium-ion batteries, Metals, 10 (2020) 316. https://doi.org/10.3390/met10030316

Werner D.M., Mütze T., Peuker U.A., Influence of cell opening methods on electrolyte removal during processing in lithium-ion battery recycling, Metals, 12 (2022) 663. https://doi.org/10.3390/met12040663

Werner S., Axel H., Die Komplexlagerstätten Tellerhäuser und Hämmerlein, 2012, ISBN: 9783981142143.

Whiteman M., Ridgway K., Particle shape discrimination using slotted sieves, Drug Development and Industrial Pharmacy, 12 (1986) 1995–2013. https://doi.org/10.3109/03639048609042621

Wilhelm T., Sygusch J., Furat O., Bachmann K., Rudolph M., Schmidt V., Parametric stochastic modeling of particle descriptor vectors for studying the influence of ultrafine particle wettability and

morphology on flotation-based separation behavior, Powders, 2 (2023) 353–371. https://doi.org/10.3390/powders2020021
Xia W., Role of particle shape in the floatability of mineral particle: an overview of recent advances, Powder Technology, 317 (2017) 104–116. https://doi.org/10.1016/j.powtec.2017.04.050

Authors' Short Biographies

Edgar Schach is a PhD candidate in Mechanical Process Engineering and Mineral Processing at the University of Freiberg, Germany. His current work focuses on battery recycling and entropy analysis of raw material processes. He previously worked at Helmholtz-Institute Freiberg for Resource Technology, where he tested new reagents for sulfide flotation, contributed to research concerning the processing of complex and finely intergrown cassiterite ores, and developed characterization techniques for multidimensional separation processes.

Dr. Thomas Buchwald got his M.Sc. in chemical engineering from the University of Applied Sciences Bremerhaven in 2016 and has since been employed at the Institute of Mechanical Process Engineering and Mineral Processing and got his PhD there at TU Bergakademie Freiberg in 2021. He is currently doing research in particle characterization and mechanical solid-liquid separation processes as well as digitization and handling of experimental data.

Dr. Orkun Furat studied Mathematics at Ulm University and received his PhD there in 2022. In his research as a postdoc at the Institute of Stochastics at Ulm University he deals with structural segmentation of tomographic image data using methods from machine learning, statistical image analysis, multidimensional probabilistic modeling based on copulas, and stochastic geometry models with a focus on morphological, textural and elemental characterization of particle systems.

Florentin Tischer is a research assistant at the Institute of particle technology at the University of Erlangen-Nuremberg, Germany. He obtained his Bachelor's degree in chemical reaction engineering and his Master's degree in particle technology at the Friedrich-Alexander-University Erlangen (Germany). His research interest is around the production of optimised polymer powders for the powder bed fusion process (additive manufacturing). This involves the use of cold wet comminution, melt emulsification and precipitation of polymers.

Alexandra Kaas is a PhD candidate at the Institute of Mechanical Process Engineering and Mineral Processing, Freiberg University of Mining and Technology, Germany. She holds a diploma degree in Mechanical Process Engineering and Particle Technology. Focusing on Potash granulation in her diploma thesis she shifted in her professional career in 2021 to the recycling of Lithium-Ion-Batteries. Alexandra is currently focusing on several projects on secondary raw material processing, such as digitalization and modelling of sorting processes.

Laura Kuger is a research associate at the Institute for Functional Interfaces (IFG) at Karlsruhe Institute of Technology (KIT) in Karlsruhe, Germany. She has a Master's degree in Bioprocess Engineering from KIT and is currently pursuing her PhD, focusing on the multidimensional fractionation of nanoparticles using magnetic field controlled continuous chromatography.

Matthias Masuhr is a PhD candidate researcher at the Institute of Technology for Nanostructures (NST) at the University of Duisburg-Essen. He has a background in Nanoengineering and Nano process technology. His research interests include nano- and submicron particles, aerosols and their classification and characterization based on multiple properties. Parts of his research were published in "Advanced Powder Technology" and at multiple conferences including European Aerosol Conference (EAC), International Congress on Particle Technology (PARTEC) and World Congress on Particle Technology (WCPT).

Johanna Sygusch studied chemistry at the Technische Universität Braunschweig and received her Master's degree in 2016 in the field of technical chemistry. Since November 2017, she has been part of the processing department of the Helmholtz Institute Freiberg for Resource Technology of the Helmholtz-Zentrum Dresden-Rossendorf. As part of her research, she investigates the surface modification and characterisation of ultrafine particles as well as the multidimensional separation of fine particulate systems via flotation.

Authors' Short Biographies

Thomas Wilhelm studied Mathematics and Economics at Ulm University and finished his Master's degree in 2021. Currently he is working as a PhD student at the Institute of Stochastics at Ulm University. His current research primarily revolves around employing machine learning techniques, statistical image analysis, multidimensional probabilistic modelling using copulas, and stochastic geometry models. The main objective of his research is to extract structural information from tomographic image data, with a specific emphasis on characterizing particle systems in terms of morphology and texture in order to optimize processes such as cooling, comminution and separation.

Dr. Ralf Ditscherlein studied physical engineering at the University of Applied Sciences in Zwickau. In his diploma thesis he dealt with the evaluation of oceanographic measurement data and was subsequently responsible for the metrological monitoring of two offshore measurement platforms in the North Sea and the Baltic Sea. In 2008, he then moved to the photovoltaic industry, where he was responsible for the coating of ceramic crucibles and the crystallization of polycrystalline silicon. Since 2017, he has been at the TU Bergakademie Freiberg at the Institute of Mechanical Process Engineering and Mineral Processing where he received his PhD in 2022 in the field of three-dimensional particle analysis using X-ray computed tomography.

Prof. Urs Alexander Peuker has been appointed Full Professor (chair) for particle technology and mineral processing in 2008 at TU Bergakademie Freiberg, Germany. In 2002 he was awarded a PhD in chemical and process engineering from the university of Karlsruhe, Germany, now KIT. From 2002 to 2008 he worked as junior professor at TU Clausthal, Germany. His main fields of work are separation processes in particle technology, mineral processing and recycling. In 2016 he became spokesman of the Priority Programme 2045 of the German Science Foundation (DFG) with the title: "Highly specific and multidimensional fractionation of fine particle systems", which was a unique possibility to have a deeper look into particle property distributions of higher dimensionality.